

SAMPLING THROUGH ITERATED APPROXIMATION: GRADIENT-FREE AND MULTI-FIDELITY BAYESIAN INFERENCE VIA TRANSPORT

DANIEL SHARP*, BART VAN BLOEMEN WAANDERS†, AND YOUSSEF MARZOUK†

Abstract. We develop an iterative framework for Bayesian inference problems where the posterior distribution may involve computationally intensive models, intractable gradients, significant posterior concentration, and pronounced non-Gaussianity. Our approach integrates: (i) a generalized annealing scheme that combines geometric tempering with multi-fidelity modeling; (ii) expressive measure transport surrogates for the intermediate annealed and final target distributions, learned variationally without evaluating gradients of the target density; and, (iii) an importance-weighting scheme to combine multiple quadrature rules, which recycles and reweights expensive model evaluations as successive posterior approximations are built. Our scheme produces both a quadrature rule for computing posterior expectations and a transport-based approximation of the posterior from which we can easily generate independent Monte Carlo samples. We demonstrate the efficiency and accuracy of our approach on low-dimensional but strongly non-Gaussian Bayesian inverse problems involving partial differential equations.

Key words. Bayesian inference, measure transport, transport maps, importance sampling, annealing, multi-fidelity.

MSC codes. 62F15, 62L99, 65M32

1. Introduction. Bayesian inference uses observational data and prior knowledge to learn or ‘calibrate’ the parameters of a mathematical model. Commonly, a scientist or engineer prescribes a computational simulation realizing the model, i.e., mapping parameters to predicted observations, and this simulation is embedded in a likelihood function that represents the conditional distribution of the data. A prior probability distribution encodes knowledge about the parameter values; this distribution is updated, via the likelihood, to produce a *posterior distribution* on the parameters of interest. The computational task of Bayesian inference is to characterize this posterior distribution—for instance, by estimating posterior expectations of arbitrary test functions. Modern methods for Bayesian computation typically grapple with three key challenges: First, the likelihood may be computationally expensive to query. Second, gradients and higher-order derivatives of this likelihood may be unavailable or computationally intractable. Third, observational data may favor narrow and geometrically complex regions of the parameter space; in this sense, the data are informative and the likelihood is strongly *concentrated* with respect to the prior.

In this paper, we introduce new computational Bayesian inference techniques for problems where all three of these challenges are central. Our focus is on problems where evaluations of the underlying simulation (and hence the likelihood) are expensive, such that one can afford at most a few hundred such queries, perhaps much less. The question of *where* in the parameter space to make these queries then becomes crucial, but the answer is complicated by the combination of posterior concentration and complex geometry. Designing queries according to the prior “wastes” model evaluations in regions of vanishing posterior probability, but placing queries in regions of high posterior probability requires not only finding these regions but describing their structure. We must therefore develop methods that capture strong non-Gaussianity, e.g., well-separated posterior modes or sharp concentration around nonlinear ridge-like structures. And while our black-box simulations do not permit gradient evaluations, these simulations often admit lower-fidelity approximations. Thus, we seek an inference framework that naturally exploits multiple model fidelities if they are available.

The core computational contribution of this paper is a novel iterative approach that uses multiple model fidelities and efficient query design to effectively neutralize the core challenges of Bayesian inference described above. In particular, our approach combines annealing, quadrature, multiple importance sampling, and variational approximations of the posterior π . In a given iteration j , we first choose a target distribution π_j using tempering (less concentrated than π) and low-fidelity modeling

*Center for Computational Science and Engineering, Massachusetts Institute of Technology, Cambridge, MA (dannys4@mit.edu, ymarz@mit.edu)

†Sandia National Laboratories, Albuquerque, NM (bartv@sandia.gov)

(cheaper to evaluate than π). We then use $\tilde{\pi}_{j-1}$, the previous iteration’s target approximation, to generate new samples or quadrature points, and apply multiple importance sampling to discretize an expectation over the current target π_j . This process draws from and augments a dataset of model evaluations accumulated over previous iterations. The resulting discretization allows us to evaluate and minimize an objective function whose minimizer is $\tilde{\pi}_j$, a variational approximation of π_j . The iterations then continue.

In related importance sampling methods, practitioners often select simple distribution approximations (which we also call *surrogates*) $\tilde{\pi}_j$, e.g., Gaussians or Gaussian mixtures, at the cost of high sampling bias and inefficiency; these issues are exacerbated by posterior concentration and complex geometry. In contrast, we use a flexible and robust *measure transport* approach to capture non-Gaussian behavior [1, 4, 30, 64, 83, 85, 101]. Moreover, our approach builds transport-based surrogates without the gradient evaluations typically required to use transport in Bayesian inference [10, 30]. Additionally, rather than using only multi-fidelity modeling or only tempering, we combine the two into a *generalized annealing process*. By integrating these notions of annealing with a versatile method to re-use evaluations of π , our approach makes particularly efficient use of expensive model evaluations, tailoring them to the geometric features of the posterior. Furthermore, our iterative scheme has a built-in robustness, described below, that mitigates the impact of a poor target approximation at any intermediate step. Synthesizing these methods yields a sequential inference approach that largely parallelizes and minimizes model evaluations, adaptively approximates the target distribution, and learns a normalized posterior density surrogate from which we sample exactly—all without gradients of the unnormalized target density.

1.1. Related work. To put our contributions in context, we outline previous methods and the extent to which they address the three challenges stated in the opening paragraph.

There is of course an enormous literature on Markov chain Monte Carlo (MCMC) methods in Bayesian computation [11, 43, 67, 69]. The first MCMC methods for expensive likelihoods trained offline surrogates for the forward model, typically by minimizing a prior-weighted approximation error [31, 65–67]. While broadly effective, these methods deteriorate under high posterior concentration [61]. Other methods have incorporated multiple model fidelities in the proposal process, via delayed acceptance schemes or multiple interacting chains [17, 45, 82]. A different class of methods create and refine surrogates for the forward model or likelihood function online, i.e., as MCMC iterations proceed [18, 20, 25, 112] possibly incorporating multi-fidelity data [108]. While all of these methods may reduce the number of expensive model evaluations, they do not necessarily ameliorate the problem of geometry. Samplers focused on challenging non-Gaussian target geometry typically require considerable information about the target density, e.g., repeated gradient and possibly Hessian evaluations [63]. Alternatively, one can attempt to “neutralize” difficult geometry of the target in various ways. Parallel tempering and simulated annealing are widely used to mitigate concentration or promote mixing between modes. More modern methods use measure transport to transform the target distribution into a distribution that is easier to sample [1, 37, 80] or, in the opposite direction, use transport to create a biasing distribution in importance sampling (IS) or a proposal in a Metropolis independence sampler [37, 70, 72, 86].

The latter methods actually straddle the line between Monte Carlo sampling and variational approximation, as their transport maps typically are built variationally. One advantage of the variational approach is that it allows embarrassingly parallel evaluations of the target distribution, which is less natural for MCMC [12, 47, 74, 92]. A fundamental problem in variational approximation, however, is the frequent use of *reverse Kullback–Leibler* (KL) divergence as an optimization objective. Minimizing reverse KL requires evaluating or estimating [84] gradients of the target log-density, but more importantly, it is intrinsically *mode-seeking*. Capturing posteriors that concentrate onto multiple modes or other non-Gaussian structures is therefore quite difficult. While there are many variational approximation schemes for Bayesian inference [8, 51, 56, 73, 85], virtually all struggle with the mode-seeking nature of reverse KL. Even using tempering for multi-modal targets does not circumvent the loss function’s basic issues [110]. A few methods use alternative loss functions to mitigate mode collapse,

avoid gradients, and improve stability [34]. Ensemble Kalman samplers represent an alternative approach to gradient-free inference but have difficulty capturing non-Gaussian posteriors [39].

Perhaps the closest methods to ours are those that iteratively create a sequence of target approximations, often involving some notion of tempering. Traditionally, these have been cast as cross-entropy methods for sequential IS [2, 16, 55, 88]. Other recent efforts try to extend the simple biasing distributions in IS by approximating other elements of the problem, and/or by using more sophisticated approximation methods. For example, [57] and [33] build quadrature- or interpolation-based surrogates of the likelihood. [57] performs tempering to iteratively refine a polynomial approximation of the forward model, using quadrature over an adapted Gaussian measure, whereas [33] interpolates on Gaussian Leja points to capture the ratios of log-likelihoods induced by models of different fidelity, without tempering. Fundamentally, both of these efforts rely on Gaussian approximations. Moreover, they do not give a posterior surrogate that one can sample in closed-form; for instance, the algorithm of [57] culminates in MCMC sampling. Yet both of these efforts provide useful inspiration for the present work, where we use multiple model fidelities and tempering, along with quadrature, to build posterior approximations more efficiently. We also rely on non-Gaussian variational approximations, found by minimizing *forward KL* rather than reverse KL, without the evaluation of likelihood gradients.

Concurrent work [52, 104] has also introduced iterative variational approximations based on forward KL minimization and tempering. As we discuss later, these schemes use accumulated samples without regard to the quality of the approximation that produced them, and thus are not robust to poor iterations in the sequence. Further, they do not emphasize sample efficiency, as demanded by expensive models; examples even in low dimensions [104] require at least 10^5 evaluations of the target. The interacting particle samplers in [68, 102] can be understood as a gradient-free tempering-based scheme, but again do not focus on parsimonious model evaluations and only return a set of samples, whereas we create a generative model for the entire posterior distribution.

1.2. Outline. In Section 2, we formalize many of the notions discussed in the introduction and propose a basic iteration for Bayesian inference via the cross-entropy method and generalized annealing. In Section 3, we describe how to create a measure transport surrogate at each iteration, identifying the surrogate using importance-weighted quadrature. In Section 4, we detail the algorithms we implement computationally: first, a more advanced strategy of “multiple tempered importance-weighted quadrature” to re-use model evaluations across iterations; and second, our full algorithmic approach, which combines the multiple tempered quadrature with multi-fidelity modeling, tempering, measure transport, and cross-entropy minimization. We comment on several algorithmic choices in Subsection 4.4, relating these choices to the broader literature. Finally, in Section 5, we demonstrate results on increasingly difficult problems: unimodal and bimodal posteriors for the source term of an elliptic PDE, a posterior over initial conditions for nonlinear convection-diffusion-reaction, and a highly concentrated posterior for inferring a parameter of a Helmholtz PDE.

2. A framework for sequential Bayesian inference. The Bayesian approach to statistical inference describes uncertainty in parameters θ probabilistically, before and after observing some data y . We work in the setting where both θ and y are real vectors that have densities with respect to Lebesgue measure. Bayes’ rule can then be written in terms of density functions:

$$(2.1) \quad \pi_{\theta|Y}(\theta|y) = \frac{\pi_{Y|\theta}(y|\theta)\pi_{\theta}(\theta)}{\pi_Y(y)} \propto \pi_{Y|\theta}(y|\theta)\pi_{\theta}(\theta).$$

We consider a fixed realization y^* of the observation and seek to approximate the posterior density $\pi_{\theta|Y}(\theta|y^*)$ in (2.1), for which we use the shorthand $\pi \equiv \pi_{\theta|Y}$.

In this section, we describe an iterative framework for building probabilistic surrogates, i.e., approximations of π . It is rooted in sequential importance sampling, though one output of our framework is a surrogate that can be used on its own, *without* importance weights. A key idea is the incorporation of tempering and multi-fidelity modeling into the iterations. Before describing novelties in sections 3 and 4, we present the fundamental framework needed to understand them.

2.1. Biasing distributions and posterior surrogates. Most often, “characterizing the posterior” amounts to computing the expectation of some function $h : \Omega \rightarrow \mathbb{R}^q$, $q \geq 1$, under the posterior π . Different choices of h correspond to, for example, the posterior mean, higher-order moments, or event probabilities. A simple and gradient-free approach to estimating such expectations is importance sampling (IS): Suppose we have identified a *biasing distribution* with density $\tilde{\pi} : \Omega \rightarrow \mathbb{R}^+$. Then the posterior expectation of h is estimated as

$$(2.2) \quad \mathbb{E}_\pi[h] = \mathbb{E}_{\tilde{\pi}} \left[h \frac{\pi}{\tilde{\pi}} \right] \approx \frac{1}{N} \sum_{i=1}^N h(\theta^{(i)}) \frac{\pi(\theta^{(i)})}{\tilde{\pi}(\theta^{(i)})},$$

where $\theta^{(i)} \stackrel{\text{i.i.d.}}{\sim} \tilde{\pi}$, and $\tilde{\pi}$ can be understood as a surrogate for the target π . This Monte Carlo estimator converges almost surely to the true expectation for integrable h under mild assumptions on $\tilde{\pi}$ and π , but the variance of the IS estimator is drastically affected by the discrepancy between $\tilde{\pi}$ and π . In particular, if $\tilde{\pi}$ assigns significantly higher probability to certain regions of Ω compared to π , the variance of the estimate can be large or even unbounded; similarly, if π assigns high probability to some region that $\tilde{\pi}$ ignores, the variance can become arbitrarily large as well. Controlling $\pi/\tilde{\pi}$, the ratio of the two densities, is then essential to good behavior of IS [78]. For simplicity, Equation (2.2) assumes that the densities π and $\tilde{\pi}$ are normalized. In practice, however, the normalization constant of π is seldom known and one must resort to a “self-normalized” version of the IS estimator (which normalizes the weights) with similar performance considerations for the biasing distribution [78]. Note that evaluating the IS estimator on the right of (2.2) crucially requires both the ability to draw samples from $\tilde{\pi}$ and to evaluate its (unnormalized) density. We therefore need to choose $\tilde{\pi}$ within a family of distributions $\mathcal{P}(\Omega)$ for which these properties hold.

We defer the discussion of good families $\mathcal{P}(\Omega)$ to Section 3 and first consider how to find $\tilde{\pi}$ within a given family. While the variance of the estimator in (2.2) can be directly related to the square of $\pi/\tilde{\pi}$, it is well established in the IS literature that a more stable objective is the log-ratio $\log \pi/\tilde{\pi}$, and hence it is useful to choose a $\tilde{\pi}$ that minimizes the *forward Kullback–Leibler* (KL) divergence:

$$(2.3) \quad \tilde{\pi}^* \in \arg \min_{\tilde{\pi} \in \mathcal{P}(\Omega)} D_{\text{KL}}(\pi \|\tilde{\pi}) = \arg \min_{\tilde{\pi} \in \mathcal{P}(\Omega)} \mathbb{E}_\pi \left[\log \frac{\pi}{\tilde{\pi}} \right] = \arg \min_{\tilde{\pi} \in \mathcal{P}(\Omega)} \mathcal{L}[\tilde{\pi}], \quad \mathcal{L}[\tilde{\pi}] := -\mathbb{E}_\pi [\log \tilde{\pi}],$$

where \mathcal{L} is the *cross-entropy loss*.¹ We note that the minimizer in (2.3) does not depend on the normalization of π . By construction, and in contrast with certain IS methods, the objective in (2.3) does not contain h , as it is intended to be robust for a wide range of posterior expectations.

If the identified $\tilde{\pi}$ is sufficiently close to π , then it is reasonable to use expectations over $\tilde{\pi}$ without IS corrections; the bias of these unweighted estimates will be sufficiently small, and the computational savings—through avoiding evaluations of the likelihood—will be significant. This is one of our goals: a key output is the surrogate itself, which allows us to draw i.i.d. samples from an approximate posterior. Importance sampling, via the iterations described next, can be seen as a means toward this goal. Using an expressive family $\mathcal{P}(\Omega)$ and accurately evaluating the loss \mathcal{L} will also be essential to achieving an accurate “standalone” $\tilde{\pi}$.

2.2. Generalized annealing. Evaluating the cross-entropy loss \mathcal{L} requires integrating over π , which we previously assumed impossible or impractical. We will approximate this expectation using IS, but through a sequence of simpler distributions that bridge between the simplicity of the prior and the complexity of the posterior π . We only create the surrogate for π at the end of this sequence. This strategy is a *generalized annealing* process, incorporating both tempering and multi-fidelity modeling.

While our approach will be applicable to generic forms of the likelihood function $\theta \mapsto \pi_{Y|\theta}(y^*|\theta)$, we first illustrate it via a likelihood that involves a computationally intensive model and additive Gaussian noise. Let $G : \Omega \rightarrow \mathbb{R}^m$ be some (generally nonlinear) function, termed the “forward model,”

¹The equivalence of minima in (2.3) is because the entropy term $\mathbb{E}_\pi[\log \pi]$ is constant with respect to $\tilde{\pi}$.

acting on parameters $\theta \in \Omega \subseteq \mathbb{R}^d$. The data are then modeled as $y = G(\theta) + \epsilon$, where $\epsilon \sim \mathcal{N}(0, \Sigma)$ with covariance matrix $\Sigma \in \mathbb{R}^{m \times m}$. This relationship yields the likelihood function:

$$(2.4) \quad \pi_{Y|\theta}(y|\theta) = \mathcal{N}(y; G(\theta), \Sigma) \propto (\det |\Sigma|)^{-1/2} \exp \left[-\frac{1}{2} (G(\theta) - y)^\top \Sigma^{-1} (G(\theta) - y) \right],$$

where the constant of proportionality is twice Archimedes' constant (i.e., 6.2831...).² Since the observation y^* is fixed, we will use the shorthand $\pi^{y^*}(\theta) := \pi_{Y|\theta}(y^*|\theta)$ for the likelihood, similar to our notation $\pi(\theta) := \pi_{\theta|Y}(\theta|y^*)$ for the posterior density.

Tempering, well-established in sampling literature [16, 41], raises the likelihood to some fractional powers $\beta \in [0, 1]$, given by an increasing sequence of *inverse temperature* parameters $(\beta_j)_{j=0}^M$ with $\beta_M = 1$. As j approaches M , the sequence of distributions $[\pi^{y^*}]^{\beta_j} \pi_\theta$ transforms from the prior distribution ($\beta = 0$) to the posterior distribution ($\beta = 1$). Since the prior is uninformed by data, we can generally view this sequence as passing from minimal concentration/maximal uncertainty to maximal concentration/minimal uncertainty. For the Gaussian noise model described above, this effect is explicit: $[\pi^{y^*}(\theta)]^\beta = \mathcal{N}(y^*; G(\theta), \Sigma/\beta)$, and hence a smaller β induces a larger covariance matrix to broaden the likelihood.

The key idea of tempered sequential IS is to use $[\pi^{y^*}]^{\beta_j} \pi_\theta$ as a biasing distribution for expectations over $[\pi^{y^*}]^{\beta_{j+1}} \pi_\theta$. For this choice to be effective, the former should cover all the high-probability regions of the latter and hence control the quantity $\log \pi/\tilde{\pi}$ discussed above. In other words, the goal is to develop points with nearly uniform (i.e., low variance) weights, taking advantage of the fact that small changes in β_j should produce small changes in density. The tempered IS construction is applied iteratively. Moreover, since sampling from $[\pi^{y^*}]^{\beta_j} \pi_\theta$ is not directly feasible, in our approach we learn biasing distributions that *approximate* the intermediate targets $[\pi^{y^*}]^{\beta_j} \pi_\theta$. The form of these iterations is detailed in Subsection 2.3.

While tempering helps address challenges of geometry, e.g., concentration of the posterior with respect to the prior, it does not reduce the computational costs of an expensive likelihood or forward model G . We will employ multi-fidelity modeling, in a similar sequential manner, to address this issue. Using the Gaussian setting of (2.4), suppose we have a sequence of forward models $(G_\ell)_{\ell=0}^L$, which define a corresponding sequence of likelihoods, $\pi_\ell^{y^*}(\theta) = \mathcal{N}(y^*; G_\ell(\theta), \Sigma)$. Here we imagine that $G_{\ell+1}$ is more “faithful” to the data-generating process than its predecessor G_ℓ , but G_ℓ is cheaper to query; e.g., G_ℓ is simulated with fewer computational degrees of freedom or involves simplified physics relative to $G_{\ell+1}$. To compute expectations over the more complicated posterior distribution induced by $G_{\ell+1}$, we use a biasing distribution built from evaluations of the cheaper model G_ℓ . For positive definite Σ and reasonable models $(G_\ell)_{\ell=0}^L$,³ the IS estimator in (2.2) will converge almost surely when using unnormalized target density $\pi_{\ell+1}^{y^*} \pi_\theta$ and unnormalized biasing density $\pi_\ell^{y^*} \pi_\theta$.

2.3. Core sequential methodology. Now we describe each iteration of our generalized annealing scheme, integrating tempering and multi-fidelity modeling with sequential IS. We define a sequence of integer fidelities and real-valued inverse temperatures $(\ell_j, \beta_j)_{j=0}^M \subset \mathbb{N} \times [0, 1]$, for steps of the generalized annealing process $j = 0, \dots, M$, satisfying $0 = \ell_0 \leq \ell_1 \leq \dots \leq \ell_M = L$ and $0 < \beta_0 < \beta_1 < \dots < \beta_M = 1$. Then we have a sequence of target distributions:

$$(2.5) \quad \pi_j(\theta) \propto \left[\pi_{\ell_j}^{y^*}(\theta) \right]^{\beta_j} \pi_\theta(\theta).$$

We will approximate each element of this sequence in succession. The target distributions $(\pi_j)_{j=1}^M$ thus induce a corresponding sequence of biasing distributions $(\tilde{\pi}_j)_{j=1}^M$, where each $\tilde{\pi}_j$ approximates π_j by minimizing the j -th cross-entropy loss $\mathcal{L}_j[\tilde{\pi}] := -\mathbb{E}_{\pi_j}[\log \tilde{\pi}]$ over biasing distributions $\tilde{\pi} \in \mathcal{P}_j(\Omega)$, where $\mathcal{P}_j(\Omega) \subseteq \mathcal{P}(\Omega)$ is some family of distributions. Crucially, each such loss is estimated via importance

²Not to be confused with π , our notation for density.

³For instance, we might assume that our domain Ω is compact and the models are bounded on Ω .

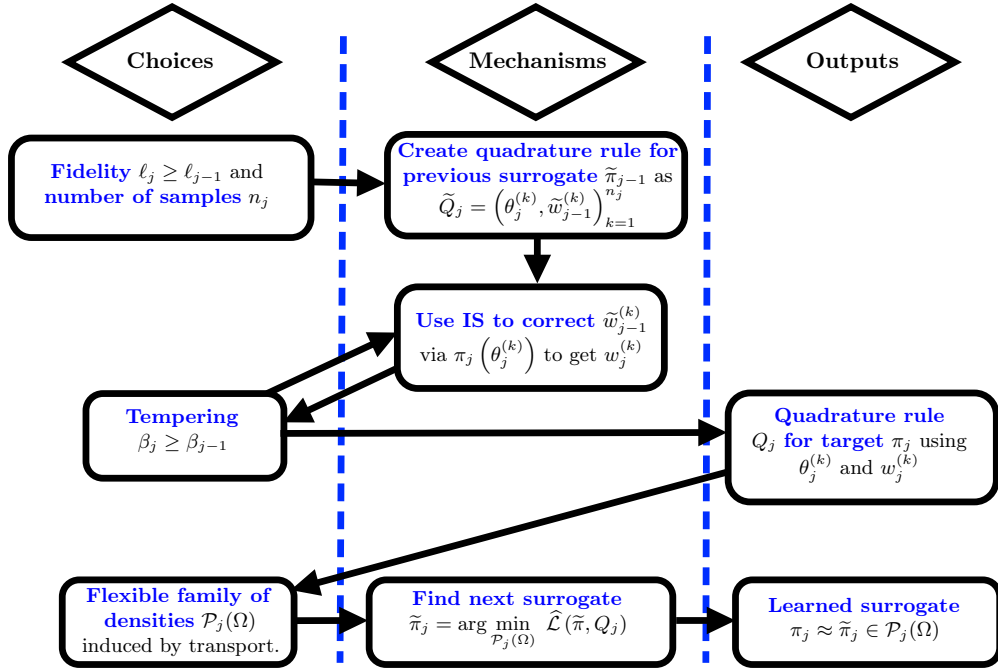


FIG. 1. Illustration of a single step j of our method, proceeding from top left to bottom right. The relationship between choosing β_j and reweighting \tilde{Q}_j is bidirectional: we select parameter β_j to ensure high-quality weights $w_j^{(k)}$.

sampling with the *previous* biasing distribution, i.e.,

$$(2.6) \quad \mathcal{L}_j[\tilde{\pi}] = - \int \log \tilde{\pi}(\theta) d\pi_j(\theta) = - \int \log \tilde{\pi}(\theta) \frac{\pi_j(\theta)}{\tilde{\pi}_{j-1}(\theta)} d\tilde{\pi}_{j-1}(\theta).$$

The next sections show how we discretize the loss \mathcal{L}_j via quadrature rules, i.e., sets of points and weights. Figure 1 is a schematic of our overall methodology, highlighting the modular steps one must take within each iteration of the sequence.

3. Measure transport. Now we discuss the families of distributions, $\mathcal{P}_j(\Omega)$, from which we select our biasing distributions $\tilde{\pi}_j$. As noted in Section 2, we must be able to sample from these biasing distributions and evaluate their densities. For good performance, and since ultimately we want $\tilde{\pi}_M$ to be an accurate standalone approximation of π , we need each $\mathcal{P}_j(\Omega)$ to include highly anisotropic, complicated distributions. For these reasons—and for additional reasons involving transformations of quadrature rules, detailed in Subsection 3.3—we construct our biasing distributions via measure transport. Transport makes the optimization in (2.3) tractable while allowing for particularly expressive surrogates. Our approach to measure transport entails the creation of deterministic *transport maps*.

3.1. Background on transport maps. A transport map $S : \Omega \rightarrow \Omega$ is, at its heart, a change of variables. Conceptually, we aim to transform a simple probability distribution η , which we are able to choose, into our given target distribution π . This *reference* distribution η , defined on Ω , is simple in the sense that we can easily sample or integrate with respect to it and that it has a tractable density; a uniform distribution on the hypercube or a Gaussian distribution are common choices. Then we choose an *invertible* transport map S to satisfy the change of variables,⁴

$$\mathbb{E}_\pi[h] = \int h(\theta) \pi(d\theta) = \int h(S^{-1}(z)) \eta(dz) = \mathbb{E}_\eta[h \circ S^{-1}].$$

⁴ U -substitution, often introduced in elementary calculus courses, is the one-dimensional analog of this transformation.

In other words, if we have a random variable $\Theta \sim \pi$ and define $Z := S(\Theta)$, then Z satisfies $Z \sim \eta$. The map S is then said to *push forward* π to η , a relationship denoted by $S_{\#}\pi = \eta$. Equivalently, if we have a random variable $Z \sim \eta$ and let $\Theta := S^{-1}(Z)$, then $\Theta \sim \pi$. We say that π is the *pullback* of η under S , denoted $S^{\#}\eta = \pi$. A map S coupling π and η in this way can always be found if π and η are absolutely continuous [101]. If S is also differentiable, then the change-of-variables yields a simple formula for the pullback density,

$$(3.1) \quad \pi(\theta) = [S^{\#}\eta](\theta) := \eta(S(\theta))|\nabla S(\theta)|,$$

where $|\nabla S(\theta)|$ is the determinant of the Jacobian of S evaluated at θ .⁵ Henceforth, we will only consider transport maps S that are invertible and differentiable. Given an invertible transport S , we can approximate posterior expectations $\mathbb{E}_{\pi}[h] = \mathbb{E}_{\eta}[h \circ S^{-1}]$ via any quadrature scheme for η . Because we choose η to allow such integration rules, but in general cannot do so with π , the map S makes these expectations tractable. For more background on measure transport, see [4, 64, 83, 101].

Now we split the problem of finding a transport map into two parts. The first question is how to choose a suitable class of invertible functions \mathcal{F} within which we will search for maps. The second question is, for a given target π , how to identify a best S within this class—i.e., an $S \in \mathcal{F}$ such that $S^{\#}\eta$ is a good approximation of π in the sense of minimizing forward KL divergence. Note that η and \mathcal{F} determine $\mathcal{P}(\Omega)$, i.e., $\mathcal{P}(\Omega) = \{S^{\#}\eta : S \in \mathcal{F}\}$. To emphasize the present contributions, we defer discussion of the first question to Section C, as there is ample previous literature on how to construct useful \mathcal{F} . Here we focus on the second question, assuming a given fixed set of candidate transports.

3.2. Cross-entropy minimization with transport. To approximate and minimize the cross-entropy loss $\mathcal{L}[\tilde{\pi}]$ over densities $\tilde{\pi}$ induced by transport maps, we first consider the generic loss in Equation (2.3). We assume that \mathcal{F} is a finite-dimensional set, each element of which is described by parameters $c \in \mathbb{R}^p$, $p < \infty$. The reference distribution η is also fixed. We then write $\tilde{\pi}(\cdot; c) = S(\cdot; c)_{\#}\eta$ for any element of $\mathcal{P}(\Omega)$. Using (3.1), minimization of the cross-entropy objective (2.3) can be written

$$(3.2a) \quad c^* \in \arg \min_{c \in \mathbb{R}^p} \mathcal{L}[\tilde{\pi}(\cdot; c)],$$

$$(3.2b) \quad \mathcal{L}[\tilde{\pi}(\cdot; c)] = -\mathbb{E}_{\Theta \sim \pi}[\log \tilde{\pi}(\Theta; c)] = -\mathbb{E}_{\Theta \sim \pi}[\log \eta(S(\Theta; c)) + \log |\nabla S(\Theta; c)|].$$

Now suppose that we have a weighted-sample approximation of expectations with respect to π , given by a quadrature rule $Q = (\theta^{(k)}, w^{(k)})_{k=1}^n$. Then we can make the approximation,

$$(3.3) \quad \mathcal{L}[\tilde{\pi}(\cdot; c)] \approx \widehat{\mathcal{L}}(c; Q) := -\sum_{k=1}^n w^{(k)} \left[\log \eta \circ S(\theta^{(k)}; c) + \log |\nabla S(\theta^{(k)}; c)| \right].$$

The choice of quadrature rule Q subsumes many common methods, e.g., Gaussian quadratures, quasi-Monte Carlo schemes. If the weights are uniform and the $\theta^{(k)}$ are drawn i.i.d. from π , then Q is a simple Monte Carlo approximation of the expectation. In this case, loss $\widehat{\mathcal{L}}$ can also be interpreted as a negative log-likelihood function, such that its minimizer c^* is a maximum likelihood estimate of the coefficients c and hence of the map $S \in \mathcal{F}$ [4, 83, 103].

In general, once the loss is discretized as in (3.3), we identify the map by minimizing $\widehat{\mathcal{L}}(c; Q)$ with respect to c ; gradients $\nabla_c \widehat{\mathcal{L}}(c; Q)$ are easily computed and a variety of gradient-based optimization algorithms can then be applied. Crucially, computing these gradients does not involve evaluating the gradient of the posterior density π . Moreover, no further evaluations of the posterior density are required during the optimization iterations.

3.3. Sequential, importance-reweighted, transport map construction. Next we bring this construction into the sequential framework described by (2.6). We replace the target π defining the cross-entropy loss \mathcal{L} above with the annealed target distribution at step j , π_j , defined in (2.5).

⁵The inverse function theorem similarly gives $S_{\#}\pi(z) = \pi(S^{-1}(z))|\nabla S(S^{-1}(z))|^{-1}$.

Now our goal is to approximate the intermediate loss $\mathcal{L}_j[\tilde{\pi}] = -\mathbb{E}_{\pi_j}[\log \tilde{\pi}]$. An expectation over π_j is generally intractable, but (2.6) converts it to an expectation over the surrogate $\tilde{\pi}_{j-1} \equiv \tilde{\pi}_{j-1}(\cdot; c_{j-1}^*)$, which approximates the previous target distribution π_{j-1} . Recalling (3.3), we thus wish to define $Q_j = (\theta_j^{(k)}, w_j^{(k)})_{k=1}^{N_j}$ for π_j given a quadrature rule for $\tilde{\pi}_{j-1}$.

Below we will show how to construct a quadrature rule $\tilde{Q}_{j-1} = (\tilde{\theta}_{j-1}^{(k)}, \tilde{w}_{j-1}^{(k)})_{k=1}^{N_j}$ for $\tilde{\pi}_{j-1}$, taking advantage of the fact that the surrogate is specified by a transport map. But first, suppose that we have such a rule. Then the cross-entropy loss (2.6) at step j becomes:

$$(3.4) \quad \begin{aligned} \mathcal{L}_j[\tilde{\pi}(\cdot; c)] &= -\mathbb{E}_{\Theta \sim \pi_j}[\log \tilde{\pi}(\Theta; c)] = -\mathbb{E}_{\Theta \sim \tilde{\pi}_{j-1}} \left[\log \tilde{\pi}(\Theta; c) \frac{\pi_j(\Theta)}{\tilde{\pi}_{j-1}(\Theta)} \right] \\ &\approx \hat{\mathcal{L}}_j(c; Q_j) := -\sum_{k=1}^{N_j} w_j^{(k)} \log \tilde{\pi}(\theta_j^{(k)}; c), \end{aligned}$$

$$(3.5) \quad = -\sum_{k=1}^{N_j} w_j^{(k)} \left(\log \eta(S(\theta_j^{(k)}; c)) + \log |\nabla S(\theta_j^{(k)}; c)| \right),$$

$$(3.6) \quad \text{where } \theta_j^{(k)} = \tilde{\theta}_{j-1}^{(k)}, \quad \nu_j^{(k)} := \tilde{w}_{j-1}^{(k)} \frac{\pi_j}{\tilde{\pi}_{j-1}}(\theta_j^{(k)}), \quad w_j^{(k)} := \frac{1}{\sum_{k=1}^{n_j} \nu_j^{(k)}} \nu_j^{(k)}.$$

Equation (3.5) comes from inserting the pullback $S^\# \eta$ from (3.2b) into $\hat{\mathcal{L}}_j$. Minimizing $\hat{\mathcal{L}}_j(c; Q_j)$ over $c \in \mathbb{R}^p$ yields the coefficients c_j^* of the surrogate $\tilde{\pi}_j(\cdot; c_j^*)$. And the weights $(w_j^{(k)})_{k=1}^{N_j}$ capture the fact that we evaluate the loss \mathcal{L}_j by *reweighing* the quadrature rule \tilde{Q}_{j-1} to produce Q_j .

We now turn to the construction of \tilde{Q}_{j-1} , the quadrature rule for the preceding surrogate distribution $\tilde{\pi}_{j-1}$. Developing deterministic quadrature schemes, e.g., Gaussian quadratures, for general multivariate distributions is difficult [38, 40, 62]. Crucially, however, our surrogate distribution is explicitly constructed as the pullback of a standard/tractable reference distribution, i.e., $\tilde{\pi}_{j-1} = S_{j-1}^\# \eta$. Let $(z^{(k)}, w_\eta^{(k)})_{k=1}^{N_j}$ be an N_j -point quadrature rule for η . We can then use the invertible map S_{j-1} to define a quadrature rule for $\tilde{\pi}_{j-1}$ as $\tilde{Q}_{j-1} = (\tilde{\theta}_{j-1}^{(k)}, \tilde{w}_{j-1}^{(k)})_{k=1}^{N_j}$ with

$$(3.7) \quad \tilde{\theta}_{j-1}^{(k)} = S_{j-1}^{-1}(z^{(k)}), \quad \tilde{w}_{j-1}^{(k)} = w_\eta^{(k)}.$$

In other words, the abscissae of the reference quadrature rule are transported and its weights are preserved [32, 94]. These abscissae and weights directly enter the expression (3.6) above, where they are reweighted to account for the mismatch between $\tilde{\pi}_{j-1}$ and π_j . Note that if the reference quadrature is unweighted independent Monte Carlo, \tilde{Q}_{j-1} amounts to i.i.d. sampling from $\tilde{\pi}_{j-1}$. But if the reference quadrature is chosen differently, as we will demonstrate in our numerical examples, the pullback quadrature can yield a more sample-efficient approximation of the loss \mathcal{L}_j .

A straightforward approach to creating the sequence $(\tilde{\pi}_j)_{j=0}^M$, as outlined in Figure 1, is to use a new reweighted pullback quadrature rule Q_j to define the loss $\hat{\mathcal{L}}_j$ at each step $j = 0, \dots, M$, with the convention $\tilde{\pi}_{-1} \equiv \pi_\theta$. The parameters c_j^* of the next biasing distribution $\tilde{\pi}_j$ are found by minimizing $\hat{\mathcal{L}}_j(\cdot; Q_j)$, and any minimizer c_j^* of this function is invariant to the normalization of π_j . Moreover, we can evaluate π_j at all N_j quadrature points in parallel; compare this with MCMC, where parallel evaluation is often impossible within a single chain. At a high level, our iterative approach connects successive steps, j and $j-1$, with importance weighting and connects each step to a common reference distribution through transport.

4. Algorithm and remarks. As a final step towards our full algorithm, we discuss a more complex method of building the quadrature rule Q_j at each step. While we can use (3.6) and (3.7) to calculate $\hat{\mathcal{L}}_j(\cdot; Q_j)$ (and its gradients) at each step, this approach naïvely discards presumably expensive evaluations of the likelihood π^{y^*} . Below, we will show that these evaluations can be actually

be re-used across tempering steps, i.e., when reweighting quadrature rules via (3.6). By reusing these evaluations, we improve the quality of our transport map approximations, which can otherwise be limited by small sample sizes. We then explore choices of the reference distribution η , list our complete algorithms, and contextualize our work on the frontier of Bayesian inference.

4.1. Multiple tempered importance-weighted quadrature. To illustrate our re-use scheme, we first consider two successive steps of the iterative algorithm described in Subsection 3.3. Let these steps have likelihoods of the same fidelity, i.e., $\ell_j = \ell_{j+1} = \ell$, but different tempering parameters $\beta_j < \beta_{j+1}$. The quadrature rule Q_j used to evaluate $\widehat{\mathcal{L}}_j(\cdot; Q_j)$ begins with a quadrature rule $\widetilde{Q}_{j-1} = (\widetilde{\theta}_{j-1}^{(k)}, \widetilde{w}_{j-1}^{(k)})_{k=1}^{n_j}$ that is then reweighted according to (3.6). Writing this process more explicitly, we first compute the *unnormalized weights* $\nu_j^{(k)}$, and then normalizing them to form Q_j :

$$(4.1) \quad \nu_j^{(k)} := \widetilde{w}_{j-1}^{(k)} \frac{(u_j^{(k)})^{\beta_j}}{v_j^{(k)}}, \quad \text{where } u_j^{(k)} := \pi_\ell^{y^*}(\theta_j^{(k)}), \quad v_j^{(k)} := \frac{\widetilde{\pi}_{j-1}(\theta_j^{(k)})}{\pi_\theta(\theta_j^{(k)})}, \quad \theta_j^{(k)} = \widetilde{\theta}_{j-1}^{(k)},$$

$$Q_j = \left(\theta_j^{(k)}, \frac{1}{W_j} \nu_j^{(k)} \right)_{k=1}^{n_j}, \quad \text{with } W_j = \sum_{k=1}^{n_j} \nu_j^{(k)}.$$

Note that this process entails n_j evaluations of the likelihood $\pi_\ell^{y^*}$. Next, we minimize $\widehat{\mathcal{L}}_j(\cdot; Q_j)$ to find a new surrogate $\widetilde{\pi}_j$ described by a transport map S_j . Via this transport, we construct a new quadrature rule $\widetilde{Q}_j = (\widetilde{\theta}_j^{(k)}, \widetilde{w}_j^{(k)})_{k=1}^{n_{j+1}}$. To obtain Q_{j+1} from \widetilde{Q}_j , we compute new unnormalized weights then normalize them:

$$(4.2) \quad \nu_{j+1}^{(k)} := \widetilde{w}_j^{(k)} \frac{(u_{j+1}^{(k)})^{\beta_{j+1}}}{v_{j+1}^{(k)}}, \quad \text{where } u_{j+1}^{(k)} := \pi_\ell^{y^*}(\theta_{j+1}^{(k)}), \quad v_{j+1}^{(k)} := \frac{\widetilde{\pi}_j(\theta_{j+1}^{(k)})}{\pi_\theta(\theta_{j+1}^{(k)})}, \quad \theta_{j+1}^{(k)} = \widetilde{\theta}_j^{(k)},$$

$$Q_{j+1} = \left(\theta_{j+1}^{(k)}, \frac{1}{W_{j+1}} \nu_{j+1}^{(k)} \right)_{k=1}^{n_{j+1}}, \quad \text{with } W_{j+1} = \sum_{k=1}^{n_{j+1}} \nu_{j+1}^{(k)}.$$

As evident from (4.2), this process evaluates $\pi_\ell^{y^*}$ at n_{j+1} new points.

Remarkably, the weights of both Q_j and Q_{j+1} use evaluations of the *same* likelihood function $\pi_\ell^{y^*}$. Rather than applying Q_{j+1} on its own, we can instead use *multiple importance sampling* [78, 100], a technique that simultaneously exploits multiple biasing distributions, to combine Q_j with Q_{j+1} . Our combined rule Q_{j+1}^{MIS} , with $N_{j+1} := n_j + n_{j+1}$ points, uses integral discretizations Q_j (with biasing distribution $\widetilde{\pi}_{j-1}$) and Q_{j+1} (with biasing distribution $\widetilde{\pi}_j$) to approximate an expectation over π_{j+1} . In other words, we obtain a quadrature rule of size $n_j + n_{j+1}$ for step $j+1$, but only evaluate the likelihood an additional n_{j+1} times. For an arbitrary function h , a multiple importance sampling estimator of its expectation over π_{j+1} is given by

$$(4.3) \quad \mathbb{E}_{\pi_{j+1}}[h] \approx \frac{1}{W_j^{\text{MIS}}} \sum_{k=1}^{n_j} \alpha_j(\theta_j^{(k)}) \nu_j^{(k)} (u_j^{(k)})^{\beta_{j+1} - \beta_j} h(\theta_j^{(k)}) + \frac{1}{W_{j+1}^{\text{MIS}}} \sum_{k=1}^{n_{j+1}} \alpha_{j+1}(\theta_{j+1}^{(k)}) \nu_{j+1}^{(k)} h(\theta_{j+1}^{(k)}),$$

where W_j^{MIS} and W_{j+1}^{MIS} are chosen to ensure a normalized quadrature rule⁶ and $\alpha_j(\theta) + \alpha_{j+1}(\theta) \equiv 1$ for any fixed input $\theta \in \mathbb{R}^d$, as in [78]. The first sum on the right-hand side of (4.3) reflects that

$$(u_j^{(k)})^{\beta_{j+1} - \beta_j} = \frac{[\pi_\ell^{y^*}(\theta_j^{(k)})]^{\beta_{j+1}}}{[\pi_\ell^{y^*}(\theta_j^{(k)})]^{\beta_j}} = \frac{[\pi_\ell^{y^*}(\theta_j^{(k)})]^{\beta_{j+1}} \pi_\theta(\theta_j^{(k)})}{[\pi_\ell^{y^*}(\theta_j^{(k)})]^{\beta_j} \pi_\theta(\theta_j^{(k)})} \propto \frac{\pi_{j+1}(\theta_j^{(k)})}{\pi_j(\theta_j^{(k)})},$$

⁶In particular, we set $W_j^{\text{MIS}} = \sum_{k=1}^{n_j} \alpha_j(\theta_j^{(k)}) \nu_j^{(k)} (u_j^{(k)})^{\beta_{j+1} - \beta_j}$ and $W_{j+1}^{\text{MIS}} = \sum_{k=1}^{n_{j+1}} \alpha_{j+1}(\theta_{j+1}^{(k)}) \nu_{j+1}^{(k)}$.

where the constant of proportionality comes from the choice of tempering parameters β_{j+1} and β_j . Note that if $(\theta_j^{(k)})_k$ and $(\theta_{j+1}^{(k)})_k$ were truly independent Monte Carlo samples (with $\theta_j^{(k)} \sim \tilde{\pi}_{j-1}$, $\theta_{j+1}^{(k)} \sim \tilde{\pi}_j$) and if $\tilde{\pi}_j$ was itself independent of the samples $(\theta_j^{(k)})_k$, then it is easy to show that (4.3) is a consistent estimator of $\mathbb{E}_{\pi_{j+1}}[h]$ [100]. In practice, however, we have created S_j by minimizing $\widehat{\mathcal{L}}(\cdot; Q_j)$, and thus Q_{j+1} is dependent on Q_j via $\tilde{\pi}_j$.

Following this two-step illustration, we now consider the general case: reusing likelihood evaluations, and hence quadrature rules Q_j , across *more* than two successive tempering steps. These quadrature rules interact through the partition of unity $(\alpha_i)_{i=0}^j$. Note that the solution of the optimization problem (3.2) is independent of the sum across all weights within Q_j^{MIS} , i.e., the loss function (3.5) is invariant to the quantity $\sum_{i=0}^j W_i^{\text{MIS}}$. Yet variance in the normalization W_i of each individual quadrature rule Q_i , for $i \leq j$, could contribute to variance in the minimizer of $\widehat{\mathcal{L}}(\cdot; Q_j^{\text{MIS}})$. We use the power heuristic $\alpha_i(\theta) \propto (n_i \tilde{\pi}_{i-1}(\theta))^\gamma$ to construct our partition of unity, where proportionality ensures a unit sum across $i = 0, \dots, j$ for any fixed value of θ . Following [100], we set the hyperparameter to $\gamma = 2$, which reweighs each surrogate according to its contribution to the variance of all the importance weights. This choice balances exploration of the domain with exploitation of areas that the current surrogates do not already fit well. We must ensure that evaluations $(u_i^{(k)})_{k=1}^{n_i}$, $i \leq j$ are from one likelihood model $\pi_\ell^{y^*}$; once we transition between likelihood fidelities, we restart the scheme. Our full *multiple tempered importance-weighted quadrature* approach is in Algorithm 4.1.

Algorithm 4.1 Multiple tempered importance-weighted quadrature

Input: Parameter β , memos $(\tilde{\pi}_i, D_i)_{i=j_0}^{j-1}$ with $D_i = \left(\pi^{y^*}(\tilde{\theta}_i^{(k)}), \tilde{\theta}_i^{(k)}, \tilde{w}_i^{(k)} \right)_{k=1}^{n_{i+1}}$

Output: Quadrature rule Q_j^{MIS} for pdf $\pi_j \propto \pi_{\ell_j}^{y^*} \pi_\theta$, where $|Q_j^{\text{MIS}}| = N_j := \sum_{i=j_0}^{j-1} n_{i+1}$

for $i = j_0, \dots, j-1$ **do**

Set $u_i^{(k)} = \pi^{y^*}(\tilde{\theta}_i^{(k)})$ and $v_i^{(k)} = \frac{\tilde{\pi}_i}{\pi_\theta}(\tilde{\theta}_i^{(k)})$ as the true and approximate likelihood weights, resp.

Define $\tilde{\alpha}_i(\theta) = (n_{i+1} \tilde{\pi}_i(\theta))^\gamma$ to weigh surrogate $\tilde{\pi}_i$ in MIS.

Define temporary weight $\tilde{\nu}_i^{(k)} = \tilde{\alpha}_i(\tilde{\theta}_i^{(k)}) \tilde{w}_i^{(k)} \frac{[u_i^{(k)}]^\beta}{v_i^{(k)}}$ for abscissa $\tilde{\theta}_i^{(k)}$.

Store point and weight $(\tilde{\theta}_i^{(k)}, \nu_i^{(k)})_{k=1}^{n_{i+1}}$ and set $W_i^{\text{MIS}} = \sum_{k=1}^{n_{i+1}} \tilde{\nu}_i^{(k)}$ as the normalization for $\tilde{\pi}_i$.

end for

For $i = j_0, \dots, j-1$, $k = 1, \dots, n_i$, set $\nu_i^{(k)} = \tilde{\nu}_i^{(k)} \left(\sum_{i'=j_0}^{j-1} \tilde{\alpha}_{i'}(\theta_i^{(k)}) \right)^{-1}$ as MIS-normalized weight.

Create final quadrature rule $Q_j^{\text{MIS}} = \bigcup_{i=j_0}^{j-1} \left(\theta_i^{(k)}, W^{-1} \nu_i^{(k)} \right)_{k=1}^{n_{i+1}}$, where $W = \sum_{i=j_0}^{j-1} W_i^{\text{MIS}}$

4.2. Choice of reference distribution. So far, we have not specified the choice of reference distribution η in our transport scheme, only requiring it to be a normalized density that we can sample from. Moreover, nothing in the algorithms above precludes the choice of reference from changing at each step; thus we may more generally write the reference at step j as η_j . Suppose, for the sake of illustration, that we could set $\eta_j = \pi_j$ (ignoring the fact that we cannot sample from this distribution and do not know its normalizing constant). Then the trivial map $S_j = \text{Id}$ would perfectly capture the target at step j . Of course this choice is impractical, but it suggests that a good choice of reference can make the minimization of $\widehat{\mathcal{L}}_j(\cdot; Q_j)$ easier and reduce the difficulty of adequately approximating S_j [83]. To this end, we propose that η_j is either the previous step's approximate posterior distribution $\tilde{\pi}_{j-1}$ or the prior distribution π_θ . The second choice is straightforward, but the first bears further discussion.

Suppose that at step $j-1$, we have found a transport map $S_{j-1}^*(\cdot) = S_{j-1}(\cdot; c^*)$ achieving $(S_{j-1}^*)^\# \eta_{j-1} = \tilde{\pi}_{j-1} \approx \pi_{j-1}$. Intuitively, if π_{j-1} and π_j are also close, then there should exist a map S_j^0 achieving $\pi_j = (S_j^0)^\# \tilde{\pi}_{j-1}$ that is close to the identity (cf. also [103, Lemma 4.5]). By setting $\eta_j = \tilde{\pi}_{j-1}$

and seeking a surrogate $\tilde{\pi}_j$ parameterized as

$$\tilde{\pi}_j = S_j^\# \tilde{\pi}_{j-1} = (S_{j-1}^* \circ S_j)^\# \eta_{j-1},$$

we effectively create a composition of transport maps. We find the new map, S_j , by minimizing $\widehat{\mathcal{L}}_j(\cdot; Q_j^{\text{MIS}})$ as described in Sections 2 and 3; at this step, the previous map S_{j-1}^* is already fixed.

We emphasize that choosing a reference distribution η_j only affects the form of $\tilde{\pi}_j$ and does not change how reweighting is performed to arrive at Q_j^{MIS} . In other words, we design Q_j^{MIS} to approximate expectations with respect to π_j , independently of the reference density η_j . To understand the difference between the choice of reference η_j and the quadrature rule Q_j^{MIS} , recall the optimization problem formulation in (3.2a). Choosing the reference changes the space of densities $\mathcal{P}_j(\Omega)$ over which we search, whereas quadrature rule Q_j^{MIS} determines the loss $\widehat{\mathcal{L}}(\cdot, Q_j^{\text{MIS}})$ that we wish to minimize.

Algorithm 4.2 Adaptive multi-fidelity multiple tempered importance-weighted quadrature

Input: Prior distribution π_θ , likelihood functions $(\pi_\ell^{y^*})_{\ell=0}^L$ of fidelity ℓ , annealing thresholds $(t_\ell)_{\ell=0}^L$ such that $0 < t_0 < t_1 < \dots < t_\ell < \dots < t_L = 1$

Output: Quadrature rule Q_M^{MIS} for π_M , transport map S_M , and reference density η_M such that $S_M^\# \eta_M \approx \pi_M \propto \pi_L^{y^*} \pi_\theta$

Initialize step counter $j = 0$, tempering parameter $\beta_{-1} = 0$, and biasing distribution $\tilde{\pi}_{-1} \equiv \pi_\theta$

for $\ell = 0, \dots, L$ **do**

 Initialize $j_0 = j$ and set $\eta_j = \tilde{\pi}_{j-1}$

do

 Record $\ell_j := \ell$

Choose n_j and create quadrature rule $\tilde{Q}_{j-1} = (\tilde{\theta}_j^{(k)}, \tilde{w}_{j-1}^{(k)})_{k=1}^{n_j}$ for integration over $\tilde{\pi}_{j-1}$

 Evaluate $u_j^{(k)} \propto \pi_{\ell_j}^{y^*}(\tilde{\theta}_j^{(k)})$ and cache $D_j = (u_j^{(k)}, \tilde{\theta}_j^{(k)}, \tilde{w}_{j-1}^{(k)})_{k=1}^{n_j}$

Choose β_j such that $t_\ell \geq \beta_j \geq \beta_{j-1}$

 Create quadrature rule $Q_j^{\text{MIS}} = (\theta_j^{(k)}, w_j^{(k)})_{k=1}^{N_j}$ from $(\tilde{\pi}_{i-1}, D_i)_{i=j_0}^j$ and β_j via **Algorithm 4.1**

 Using information on Q_j^{MIS} and η_j , **choose** regularizer λ_j and function class \mathcal{F}_j for map $S_j(\cdot; c)$

 Find parameters $c^* \in \arg \min_c \widehat{\mathcal{L}}(c; Q_j^{\text{MIS}}) + \lambda_j \|c\|^2$

 Set $\tilde{\pi}_j = S_j(\cdot; c^*)^\# \eta_j$, $\eta_{j+1} = \pi_\theta$, and increment j

while $\beta_j < t_\ell$

end for

Record maximum step $M = j$

4.3. Complete algorithm. Algorithm 4.2 formalizes the multi-fidelity inference method illustrated in Figure 1 and detailed in Sections 2–4.2. The algorithm is fully described by γ , $(t_\ell)_{\ell=0}^L$, $(\beta_j)_{j=0}^M$, $(n_j)_{j=0}^M$, $(\lambda_j)_{j=0}^M$, and $(\mathcal{F}_j)_{j=0}^M$. Several of these hyperparameters are chosen in-the-loop, as emphasized by boldface type in Algorithm 4.2. Our choices for setting these parameters are as follows.

As ℓ_j (the likelihood fidelity level at step j) increases, the number of likelihood evaluations n_j should be chosen according to the expense of the likelihood $\pi_{\ell_j}^{y^*}$, as suggested earlier. The threshold sequence $(t_\ell)_{\ell=0}^L$ defines the range of inverse temperature parameters β_j than can be used for a given fidelity; we enforce $t_{\ell-1} \leq \beta_j \leq t_\ell$ for steps j employing likelihood fidelity ℓ , so that higher-fidelity models are deployed as we get closer to the final distribution, i.e., as $\beta_j \rightarrow 1$. The choice of transport map function class \mathcal{F}_j is intricately tied to the choice of quadrature rule and reference distribution. On the one hand, setting the reference to be the previous surrogate/pullback distribution, $\eta_j = \tilde{\pi}_{j-1}$, may give an easier approximation problem as described in Subsection 4.2; on the other hand, the resulting composition of transport maps can overfit to the sparse data in Q_j^{MIS} . Such overfitting may motivate

the use of more advanced adaptive transport map parameterizations in the future [4], but here we use the simple rule for choosing η_j in Algorithm 4.2, which is demonstrated to be effective in Section 5: Every time a new fidelity is chosen, we set the reference to be the previous surrogate, $\eta_j = \tilde{\pi}_{j-1}$; then, after the first surrogate is found for a given fidelity, we set $\eta_j = \pi_\theta$.

To choose β_j within its allowable range at each step and to adjust the complexity/size of \mathcal{F}_j , we compute the relative effective sample size (rESS) of the current quadrature. For any quadrature rule Q with weights $\mathbf{w} = (w^{(1)}, \dots, w^{(N)})$, we define $\text{rESS}[Q] = (N\|\mathbf{w}\|_2^2)^{-1}$ as an a priori indicator of error. When the weights are positive and sum to one, the rESS takes a value in $[N^{-1}, 1]$, where a rESS of unity is desirable but does not guarantee high-quality integration. If the rESS is small, many of the weights of Q are near zero; if the rESS is large, the samples are weighted nearly uniformly and thus Q resembles a (quasi-)Monte Carlo quadrature. When the set of transport maps \mathcal{F}_j admits high-frequency functions, we avoid overfitting by using $\text{rESS}[Q_j^{\text{MIS}}]$ to guide the choices of β_j and \mathcal{F}_j . In general, we tune \mathcal{F}_j to be simpler for low values of rESS. The tempering parameters $(\beta_j)_j$ are chosen via the systematic scheme detailed in Section B. At a high level, this approach uses a simple (e.g., low-degree) class of functions \mathcal{F}_j and takes only small increments of the tempering parameter β_j (i.e., small $\beta_j - \beta_{j-1}$) when the rESS diagnostic is small. Conversely, we allow for larger function classes \mathcal{F}_j and larger increases $\beta_j - \beta_{j-1}$ when the rESS is larger. The L^2 regularization hyperparameters $(\lambda_j)_{j=0}^M$ further regularize the transport map parameters; we find it necessary to include a regularization term for stability, but our results are insensitive to the choice of small regularization.

4.4. Algorithmic insight. Though we already discuss related work in Subsection 1.1, we can now comment more precisely on certain aspects of our algorithm. First, recall the comparison with [33, 57], which also consider the problem of highly concentrated posterior distributions. As noted earlier, a key distinction from these earlier works is the output of our algorithm: we create an expressive transport-based surrogate $\tilde{\pi}_M$ (which provides both a normalized density estimate and a fast i.i.d. sampler) and an approximate quadrature rule Q_M for the distribution π_M . In contrast, [57] creates a *Gaussian* approximation of π and a polynomial approximation of the forward model; sampling from the posterior approximation induced by this forward model surrogate is then left to MCMC. [33] uses multi-level sparse grids to create both an interpolation of the log-likelihood and a quadrature rule over an adapted Gaussian measure, but this approach is again limited by its Gaussian assumption and cannot handle strongly multi-modal targets.

More broadly, in Algorithm 4.2 we have specified a method with many building blocks. These building blocks are largely modular: to demonstrate our algorithm, we implement particular choices for each element, but these choices are not prescriptive or totemic. Rather, we see our core contribution as the framework (generalized annealing, variational construction of transport, multiple tempered importance-weighted quadrature) within which all these elements interact. One such building block is the choice of quadrature family and transport class. We find better results with non-deterministic quadrature rules, specifically randomized QMC, rather than deterministic rules. Our transports are parameterized by monotone polynomials, as detailed in Section C. Several recent papers [32, 48, 53, 60] have specifically studied the construction of quadrature via transport, though in contrast with some of these efforts, we use quadrature to identify transport maps (by discretizing a variational objective) *and* we use transport to create new quadrature rules, rather than doing only the latter. [60] investigates the construction of transport maps specifically tailored to randomized QMC, by enforcing certain smoothness and growth rate conditions.

Another building block is the scheme for choosing a tempering schedule $(\beta_j)_{j=0}^M$. This is a widely studied problem, with many common heuristics and even some theory, e.g., ‘optimal’ schedules for a fixed integrand [15, 95]. Here we have taken a practical approach, modifying the schemes in [59, 104]⁷ as described in section B. But many other tempering schedules could be incorporated in our framework. Also, while there is ample previous work on multi-fidelity methods in importance sampling [81, 82, 89], the use of multi-fidelity models with tempering is less widespread [89]. Very recent work [13] lends

⁷These works independently proposed virtually identical methods.

theoretical support to our heuristic of picking more complex models at higher inverse temperatures.

It is interesting to contrast the computational patterns of minimizing the cross-entropy (forward KL) loss \mathcal{L} , as we do here, with those of reverse KL minimization, often used in variational inference. We incur one forward model or likelihood evaluation for each quadrature point used to approximate \mathcal{L} ; optimization iterations then involve no new model evaluations. In contrast, reverse KL minimization requires re-evaluating the model at new quadrature points every time the transport map changes (since the reverse KL integrates over the changing pullback distribution instead of over the static target). Also, the cross-entropy loss function \mathcal{L} is well-known to be *moment-matching*, so any minimizer $\tilde{\pi}(\cdot; c^*)$ will tend to have similar expectations as π . On the other hand, reverse KL minimization is *mode-seeking*, which generally yields poor approximations of multi-modal targets [34] and has been described as inadequate for importance sampling [49].

An alternative to variational approximation of transports is given by the tensor-based transport methods of [21–23, 27], which *interpolate* the unnormalized target density and then explicitly approximate the associated Knothe–Rosenblatt transport map via tensor-based integration. Some of these methods also employ a sequence of bridging densities. See [22] for a comparison to cross-entropy methods. *Deep* tensor methods are necessarily constructed as a composition of maps. Empirically, we observe numerical instability when composing more than a few maps, i.e., choosing $\eta_{j+1} = \tilde{\pi}_j$ for more than one or two consecutive steps. This difference may be due to the interpolation property of tensor methods, compared to our variational procedure.

To our knowledge, no theory characterizes the convergence of Q_j^{MIS} in Algorithm 4.1, particularly when these quadrature rules are employed iteratively in the context of a cross-entropy method. Nevertheless, the re-use of expensive likelihood evaluations is crucial in the small-sample setting of interest here. Our weighting of different biasing distributions as in Algorithm 4.1 extends the unweighted mixing of datasets suggested in contemporaneous work [52, 104]. In particular, the partition of unity α_j in our scheme makes the different transport maps mix according to how well they “trust” one another, i.e., how close the surrogate distributions are to one another when evaluated at the quadrature points. This mixing emulates characteristics of defensive importance sampling [44, 76] as well as some behavior of *contrastive learning* [5]. Samples in Q_j^{MIS} not only help the transport map approximate the posterior where it is concentrated but also reveal where little posterior mass is present.

5. Numerical examples. All forward models are implemented in the open-source MrHyDE toolkit [106] and transport maps using the MParT package [79].⁸ Our forward models are induced by various parametric partial differential equations (PDEs), each described in the ensuing subsections. The parameters θ of each PDE are endowed with a uniform prior on the d -dimensional hypercube $[0, 1]^d$, for values of d specified below. To integrate over this uniform distribution, we use the randomized QMC method described in Section A. The likelihood function is of the form (2.4) with isotropic Gaussian observation errors. In particular, we define a hierarchy of forward models $(G_\ell)_{\ell=0}^L$ with $G_\ell : [0, 1]^d \rightarrow \mathbb{R}^m$ and $\pi_\ell^{y^*}(\theta) \propto \exp(-\frac{1}{2\sigma_\ell^2} \|G_\ell(\theta) - y^*\|^2)$ with $\pi_\theta(\theta) \equiv 1$. Choosing target model G_L gives $\pi_L^{y^*}$ as our highest fidelity likelihood, so $\ell_M = L$ and $\ell_0 = 0$.

The PDEs in the examples below are all defined on the domain $\mathcal{X} = [0, 1]^2$ (where this spatial dimension should not be confused with the parameter dimension d). The data $y^* \in \mathbb{R}^m$ correspond to observations of the PDE solution at m points in \mathcal{X} . To avoid an “inverse crime” [50], we generate y^* from a higher-fidelity PDE solution than G_L (i.e., a finer spatial/temporal discretization) and, unless otherwise stated, add noise to these observations. In our multi-fidelity examples below, we use tempering thresholds $(t_1, t_2) = (0.5, 0.8)$, i.e., increase the fidelity when $\beta_{j-1} \geq 0.5$ and again when $\beta_{j-1} \geq 0.8$. We denote the number of new model evaluations at step j by n_j and the parameter count in the biasing distribution $\tilde{\pi}_j$, i.e., the dimension of \mathcal{F}_j , by p_j . Overall, we seek to use these four examples to demonstrate the different characteristics we seek for Bayesian computational approaches: accurate posterior density approximation without gradients, robustness to unusual concentration and

⁸Code to reproduce all examples is available at <https://github.com/dannys4/MultilevelTransport>.

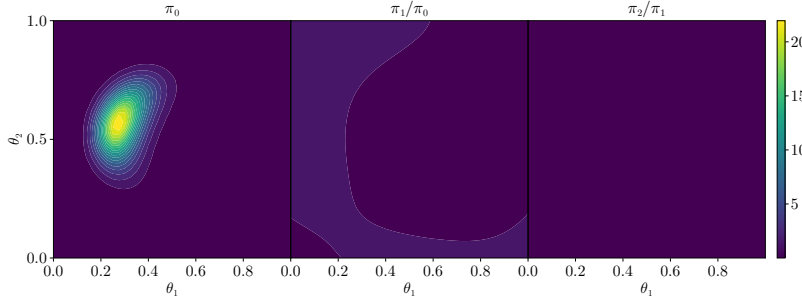


FIG. 2. Likelihood ratios induced by the three PDE discretizations in Subsection 5.2.

mode separation, resilience to poor intermediate approximations, and a balance between exploration and exploitation for quadrature with a limited budget.

5.1. Error metrics. We quantify the error at step j four ways. To assess the error in each quadrature rule Q_j^{MIS} relative to π_M , we report the error in the mean (RMSE), defined as $D(\pi_M, \tilde{\pi}_j) = \|\mathbb{E}_{\pi_M}[\Theta] - \hat{\mu}(Q_j^{\text{MIS}})\|_2$, where $\hat{\mu}(Q) = \sum_{k=1}^N w^{(k)} \theta^{(k)}$ for a quadrature rule $Q = (\theta^{(k)}, w^{(k)})_{k=1}^N$. Similarly, we compute the covariance matrix of Θ using Q_j^{MIS} and report the Förstner distance [36] (the geodesic distance on the symmetric positive-definite manifold) between this approximation and the true covariance. To quantify the discrepancy between surrogate density $\tilde{\pi}_j$ and the target high-fidelity posterior π_M , we estimate the maximum mean discrepancy (MMD) [71] between the two, with the squared-exponential and Matérn-1.5 kernels; these errors are denoted MMD_G and $\text{MMD}_{\text{M1.5}}$, respectively. Thus, we quantify error of Q_j^{MIS} in two ways and measure the error of $\tilde{\pi}_j$ in two ways. For each of these four error discrepancies, labeled $D(\cdot, \cdot)$, we report $D(\tilde{\pi}_j, \pi_M)/D(\pi_\theta, \pi_M)$. This relative scaling to ensures that, even if the prior is a good approximation to the posterior, we still improve on it. See the supplementary material’s Section F for a more thorough discussion of our error metrics, including the computation of “reference” values of the posterior moments.

5.2. Diffusion single-source inversion. As in [33], we start with the elliptic PDE

$$(5.1) \quad \Delta u = A(\alpha) \exp\left(-\frac{1}{2\alpha^2} \|\mathbf{x} - \theta\|^2\right), \quad u(\mathbf{x}) \equiv 0, \quad \mathbf{x} \in \partial\mathcal{X},$$

where $A(\alpha) = \frac{5}{\tau\alpha}$ and $\alpha = 0.15$, with τ twice Archimedes’ constant. This is a simple example with a linear PDE and $d = 2$, but nonetheless offers algorithmic insight due to its concentrated non-Gaussian posterior. We use 16 observations at $(0.2i, 0.2j)$ for $i, j \in \{1, 2, 3, 4\}$, with noise variance $\sigma^2 = 0.04$. We define our models using successively finer meshes in a finite-element solver. For more details on discretizations and solvers in all examples, see Section G. In Figure 2, we compare the likelihoods $\pi_0^{y^*}$, $\pi_1^{y^*}$, $\pi_2^{y^*}$ and see diminishing returns as we increase fidelity; $\pi_1^{y^*}$ is quite close to $\pi_2^{y^*}$.

Table 1 shows hyperparameters and numerical results of running our algorithm. Visualizations of π_j , $\tilde{\pi}_j$, and $\pi_j \log \frac{\pi_j}{\tilde{\pi}_j}$ (i.e., the integrand in the KL divergence) are given in Figure 4. We see that the surrogate density and samples closely match the desired target. We also show, in Figure 3, a few of the quadrature rules Q_j^{MIS} produced by the algorithm. Recall the discussion of reference choice in subsection 4.2; the interplay between the reference η_j and family of densities \mathcal{F} can be seen in the choice of p_j , where we choose a smaller p_j on the steps that ℓ increases. We re-emphasize that not only do we capture quantities of scientific interest (reflected by the RMSE in the mean and Förstner error in the covariance), but our overall error decreases continually with a small evaluation budget. This example demonstrates that we can efficiently and accurately capture the target density using Algorithm 4.2 with only 175 model evaluations: simulating the low, medium, and high-fidelity models 100, 25, and 50 times, respectively.

5.3. Diffusion multi-source inversion. We now tackle the bimodal experiment from [33]

$$(5.2) \quad \Delta u = A(\alpha) \exp\left(-\frac{1}{2\alpha^2} \|\mathbf{x} - \theta\|^2\right) + bA(\alpha) \exp\left(-\frac{1}{2\alpha^2} \|\mathbf{x} - \nu\|^2\right); \quad u(\mathbf{x}) \equiv 0, \quad \mathbf{x} \in \partial\mathcal{X},$$

TABLE 1

Hyperparameters and error metrics for Subsection 5.2. Row j corresponds to Q_j^{MIS} and $\tilde{\pi}_j$. $n_j = 25$ at each step.

Hyperparameters				Error Metrics				
j	ℓ_j	β_j	p_j	rESS	RMSE	Förstner	$\text{MMD}_{\text{M}_{1.5}}$	MMD_{G}
0	1	0.125	14	8.20×10^{-1}	6.78×10^{-1}	8.94×10^{-1}	8.88×10^{-1}	8.93×10^{-1}
1	1	0.250	14	6.61×10^{-1}	4.70×10^{-1}	7.15×10^{-1}	7.76×10^{-1}	7.86×10^{-1}
2	1	0.400	20	5.36×10^{-1}	2.81×10^{-1}	5.29×10^{-1}	6.32×10^{-1}	6.44×10^{-1}
3	1	0.500	20	5.19×10^{-1}	2.21×10^{-1}	4.19×10^{-1}	5.41×10^{-1}	5.54×10^{-1}
4	2	0.800	9	6.06×10^{-1}	3.12×10^{-2}	4.62×10^{-2}	8.17×10^{-2}	8.12×10^{-2}
5	3	1.000	9	9.50×10^{-1}	8.00×10^{-2}	6.00×10^{-2}	1.65×10^{-1}	1.69×10^{-1}
6	3	1.000	35	9.31×10^{-1}	6.33×10^{-2}	7.88×10^{-2}	1.38×10^{-1}	1.40×10^{-1}

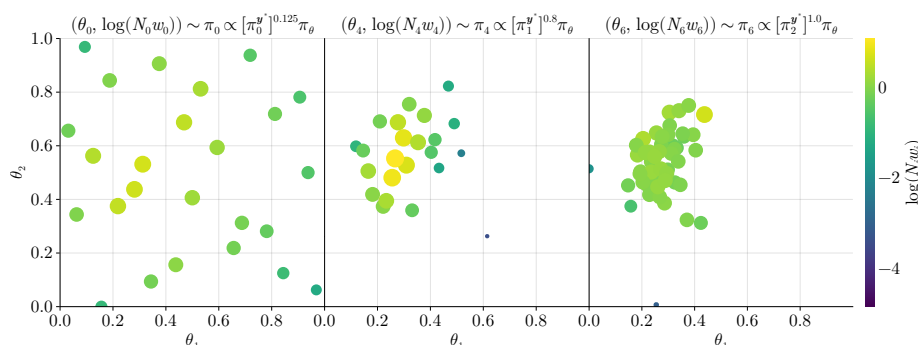


FIG. 3. Quadrature rules Q_j^{MIS} for Subsection 5.2. Both color and size reflect the weight of a point, with uniform weights desired.

where $b \in \{0, 1\}$ dictates whether we evaluate the PDE or generate data, respectively: we use two localized sources to generate data but a single-source parameterization of the right-hand side (cf. Subsection 5.2) when performing inference. The data is generated using $\theta = (0.15, 0.15)$ and $\nu = (0.85, 0.85)$. To preserve strong bimodality and interesting features of the target density, we add no observation noise to generate y , observed at the same sensor locations as Subsection 5.2. Ratios of the successive likelihoods are visualized in Figure 5. As the prior and true posterior have identical mean $(0.5, 0.5)$, we report the average of Q_j^{MIS} instead of RMSE. Quantitative results of our algorithm are in Table 2 and the final approximation $\tilde{\pi}_M$ of the target distribution is visualized in Figure 6. The column of Table 2 labeled $\tilde{\mu}_j$ shows the quadrature approximation of the posterior mean via Q_j^{MIS} at each step; these values should be compared to the true mean, $(0.5, 0.5)$.

The performance of our algorithm improves significantly on results from [33]; we capture multimodal behavior with only $p_M = 35$ parameters in the density surrogate $\tilde{\pi}_M$. By contrast, [33] fails to accurately capture multi-modality even with $O(100)$ parameters in its interpolant, demonstrating that the dataset used to construct the surrogate (here, our Q_M^{MIS} , in the bottom left of Figure 6) is the crucial factor, not the complexity of the surrogate itself. In this example, we see a continual decrease in errors; in fact, the final MMD and covariance errors relative to the high-fidelity posterior are on the order of 10^{-1} , but we only use 75 high-fidelity posterior evaluations and 175 total model evaluations. Errors in the mean (compared to the true value) are on the order of 10^{-2} . For comparison, if we could hypothetically draw 75 independent and unweighted Monte Carlo samples from π_M directly (which of course is not possible), the resulting Monte Carlo standard error in the mean estimate would be approximately 3.42×10^{-2} . Thus, our algorithm performs comparably to or better than perfect Monte Carlo sampling of π_M ; compare this to the asymptotic bias in [33, Figure 7].

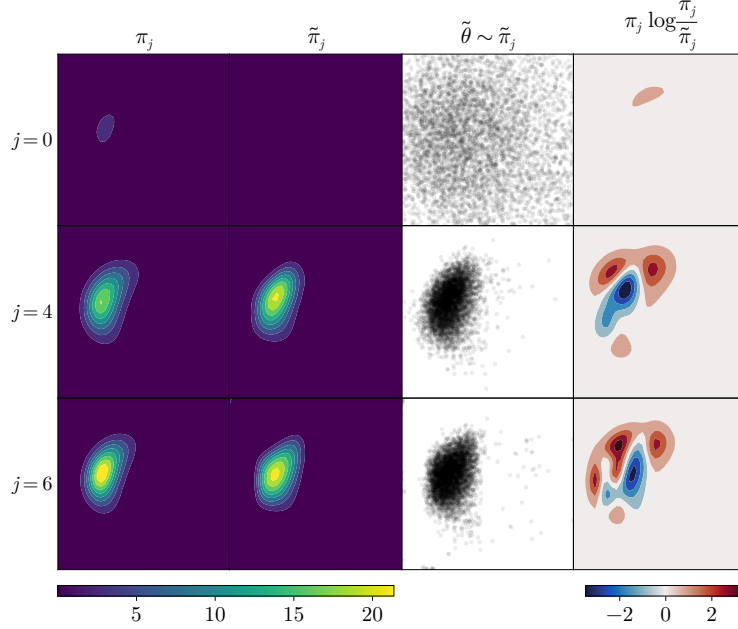


FIG. 4. Visualizing the results for Subsection 5.2. Columns from left to right: target density π_j , transport-induced surrogate density $\tilde{\pi}_j$, samples from the surrogate, and weighted log-ratio of π_j to $\tilde{\pi}_j$.

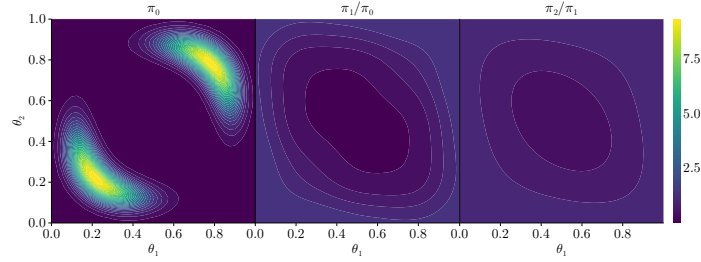


FIG. 5. Likelihood ratios induced by the three PDE discretizations in Subsection 5.3.

TABLE 2
Hyperparameters and error metrics for Subsection 5.3. Row j corresponds to Q_j^{MIS} and $\tilde{\pi}_j$.

j	Hyperparameters			Error Metrics					
	ℓ_j	β_j	p_j	rESS	$\tilde{\mu}_j$	Förstner	$\text{MMD}_{\text{M}_{1.5}}$	MMD_{G}	
0	1	0.200	14	8.21×10^{-1}	0.487	0.504	8.99×10^{-1}	9.63×10^{-1}	9.66×10^{-1}
1	1	0.325	27	6.63×10^{-1}	0.476	0.488	6.58×10^{-1}	6.38×10^{-1}	6.46×10^{-1}
2	1	0.500	27	5.38×10^{-1}	0.462	0.499	4.86×10^{-1}	4.95×10^{-1}	5.02×10^{-1}
3	2	0.800	9	6.27×10^{-1}	0.521	0.526	4.55×10^{-2}	4.51×10^{-1}	4.59×10^{-1}
4	3	1.000	9	7.18×10^{-1}	0.466	0.479	4.16×10^{-2}	4.23×10^{-1}	4.32×10^{-1}
5	3	1.000	27	6.83×10^{-1}	0.469	0.469	4.16×10^{-2}	2.41×10^{-1}	2.45×10^{-1}
6	3	1.000	35	7.52×10^{-1}	0.470	0.481	4.30×10^{-2}	1.94×10^{-1}	1.95×10^{-1}

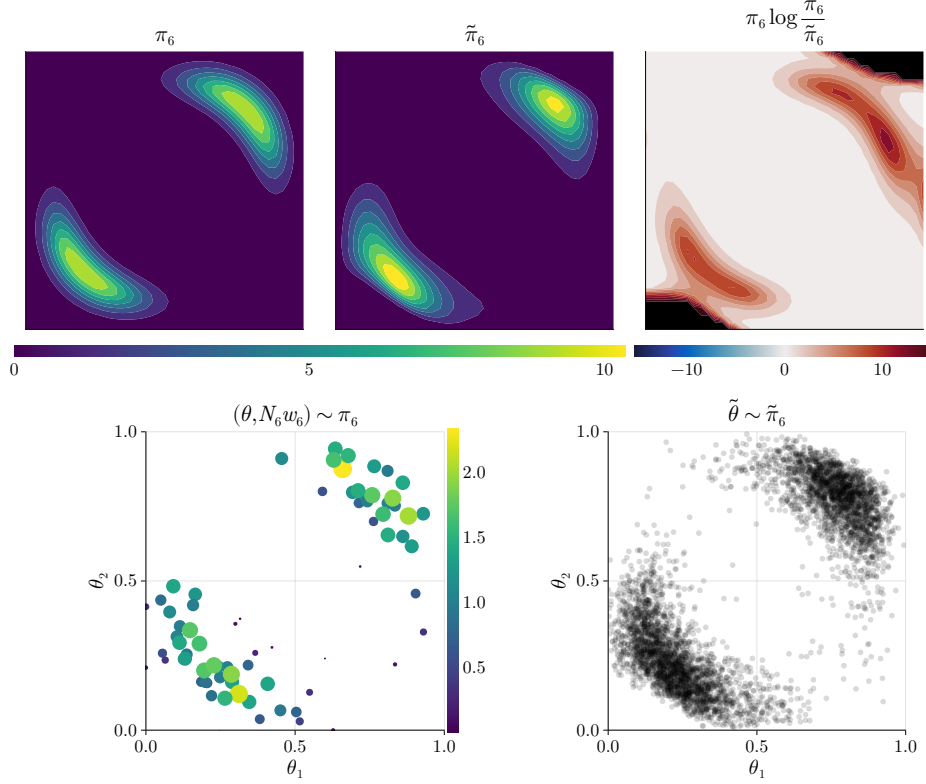


FIG. 6. Visualizing the results for Subsection 5.3. (Top): From left to right, we compare the truth, surrogate, and KL integrand (where a black region for the KL integrand corresponds to when $\tilde{\pi}_M(\theta) = 0$ numerically). (Bottom left): Final quadrature Q_M^{MIS} . (Bottom right): Samples from the pullback distribution $\tilde{\pi}_M$.

5.4. CDR initial condition inversion.

Consider the convection-diffusion-reaction PDE,

$$(5.3) \quad \begin{aligned} \frac{\partial u}{\partial t} - \nabla \cdot (\kappa \nabla u) - \mathbf{c}_\ell \cdot \nabla u - 5u^2 &= 0 \quad \forall \mathbf{x} \in \mathcal{X}, t \in (0, 10]; \quad u(t, \mathbf{x}) \equiv 0 \quad \forall \mathbf{x} \in \partial \mathcal{X}, t \in (0, 10] \\ u(0, \mathbf{x}) &= A(\alpha) \left[\exp\left(-\frac{4}{2\alpha^2} \|\mathbf{x} - \mathbf{x}_1\|^2\right) + \exp\left(-\frac{1}{2\alpha^2} \|\mathbf{x} - \mathbf{x}_2\|^2\right) \right] \quad \forall \mathbf{x} \in \mathcal{X}. \end{aligned}$$

We use zero-Dirichlet conditions on the top and left boundaries and zero-Neumann conditions on the right and bottom boundaries. We wish to infer the initial condition of this nonlinear and time-dependent PDE, parameterized by $\theta = (\mathbf{x}_1, \mathbf{x}_2) \in [0, 1]^4$, from observations that are sparse in both space and time. The data-generating parameters are $\mathbf{x}_1^{\text{true}} = (0.6, 0.85)$ and $\mathbf{x}_2^{\text{true}} = (0.15, 0.40)$. Here, we keep constant mesh sizes across the levels j and instead model the Peclet number as increasing across fidelities ℓ . We impose this using velocity vectors of increasing magnitude, $\mathbf{c}_\ell \equiv \frac{\ell}{2}(1, -1)$ for $\ell = 0, 1, 2$, where data for inference are generated at $\mathbf{c}^{\text{true}} \equiv \mathbf{c}_2$. Our observations are taken at the same spatial locations as in the previous two examples, tensorized with six observation times $t \in \{0.5, 0.6, \dots, 1\}$. The PDE solution u obtained with the true convective term \mathbf{c}_2 is pictured in Figure 7. In Figure 8, we visualize one- and two-dimensional marginals of the target distributions π_0 , π_1 , and π_2 . These plots demonstrate that the modes deform nonlinearly as the convection speed increases.

Hyperparameter values for our algorithm and error metrics over successive iterations are reported Table 3, where we choose $n_j = 75$ for this higher-dimensional example. Samples and marginal densities of $\tilde{\pi}_M$ are shown in Figure 9. Because the errors in Table 3 are relative, their scale is not affected by the parameter dimension d . We do see slightly slower reduction of the error with the number of samples compared to the prior examples, which is expected for several reasons. The larger parameter

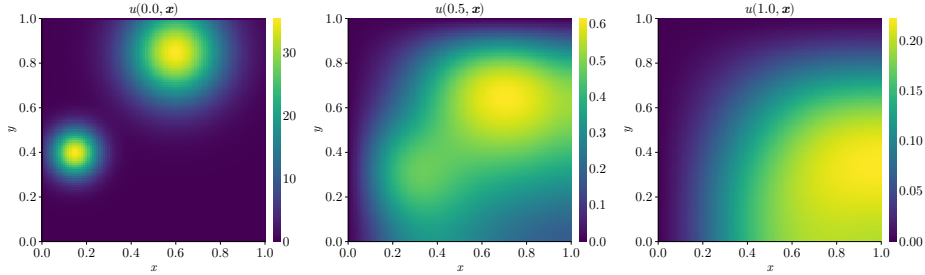


FIG. 7. Solution to PDE (5.3) for given convection $\mathbf{c}^{\text{true}} = \mathbf{c}_2 = (0.5, -0.5)$ at time snapshots $t = 0, 0.5, 1$.

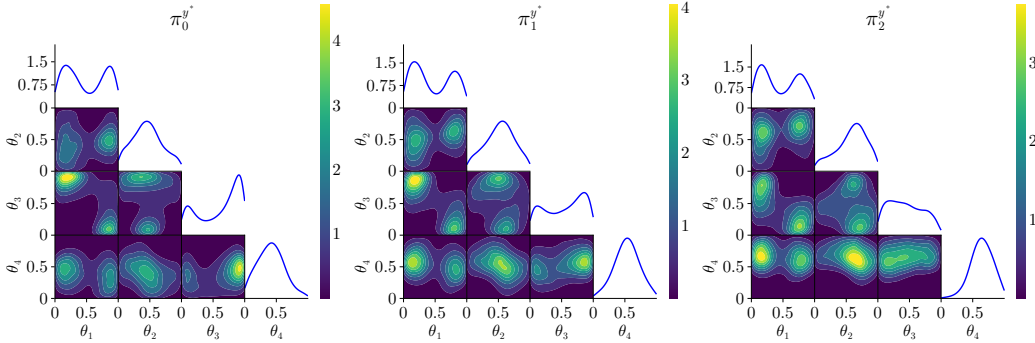


FIG. 8. Kernel density estimators (KDEs) of likelihood marginals in Subsection 5.4 for each fidelity.

TABLE 3
Hyperparameters and error metrics for Subsection 5.4. Row j corresponds to Q_j^{MIS} and $\tilde{\pi}_j$. $n_j = 75$ at each step.

j	Hyperparameters			Error Metrics				
	ℓ_j	β_j	p_j	rESS	RMSE	Förstner	$\text{MMD}_{\text{M}1.5}$	MMD_{G}
0	1	0.300	34	8.22×10^{-1}	1.24×10^0	8.19×10^{-1}	1.01×10^0	1.01×10^0
1	1	0.500	125	6.64×10^{-1}	1.49×10^0	6.67×10^{-1}	1.11×10^0	1.11×10^0
2	2	0.675	69	5.33×10^{-1}	9.06×10^{-1}	6.12×10^{-1}	9.47×10^{-1}	9.69×10^{-1}
3	2	0.800	125	5.02×10^{-1}	9.67×10^{-1}	4.38×10^{-1}	9.09×10^{-1}	9.34×10^{-1}
4	3	0.800	34	2.29×10^{-1}	3.93×10^{-1}	8.04×10^{-1}	7.44×10^{-1}	7.87×10^{-1}
5	3	0.800	125	4.05×10^{-2}	1.37×10^0	1.09×10^0	2.09×10^0	2.33×10^0
6	3	0.800	329	3.15×10^{-1}	5.21×10^{-1}	8.34×10^{-1}	7.72×10^{-1}	8.38×10^{-1}
7	3	0.800	329	2.64×10^{-1}	4.24×10^{-1}	7.10×10^{-1}	7.86×10^{-1}	8.49×10^{-1}
8	3	1.000	329	5.66×10^{-1}	3.79×10^{-1}	7.87×10^{-1}	7.89×10^{-1}	8.46×10^{-1}

dimension d (i) leads to larger errors in our quadrature approximation for the same number of model evaluations, and (ii) requires searching within larger classes of functions $(\mathcal{F}_j)_j$ for our transport maps. Additionally—by construction—this example contains significantly more model mismatch between successive fidelities, compared to the previous examples. Thus when we transition from an intermediate Peclet number model to the final model at step $j = 4$, our biasing distribution proposes inefficient and somewhat uninformative samples. Nevertheless, we are able to correct for the bias in the low-fidelity models and efficiently capture the final target distribution’s multi-modality and anisotropy with relatively few evaluations: compare the rightmost axes in Figures 8 and 9.

The reduction of error from step $j = 5$ to $j = 6$ demonstrates robustness to poor intermediate surrogates, due to our multiple IS procedure: the weighting step in multiple IS allows us to recognize the

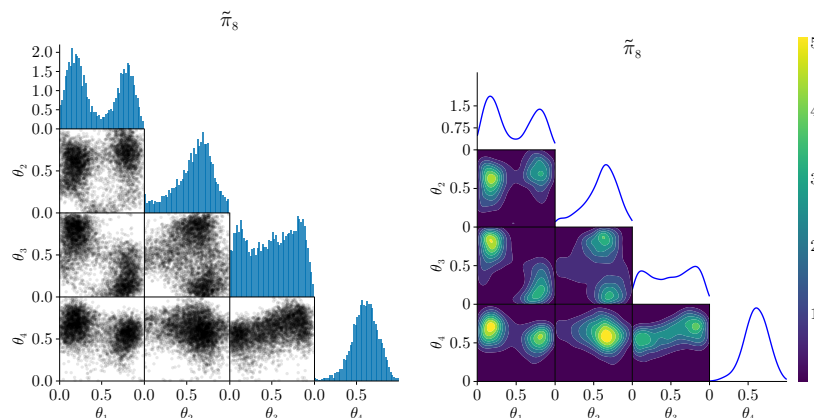


FIG. 9. Visualization of the results for Subsection 5.4. (Left): samples $\tilde{\theta} \sim \tilde{\pi}_8$ with one-dimensional histograms on the diagonal. (Right): KDE of the two-dimensional marginals of $\tilde{\pi}_8$ with one-dimensional KDE on the diagonal.

poor efficiency of the rule Q_5 and defensively rely on samples from steps $j = 4$ and $j = 6$. We find that this reweighting approach, not present in [52, 104], prevents the algorithm from diverging due to poor intermediate approximations, and is vital to Bayesian inference with small model evaluation budgets and in multi-fidelity settings where differences between available models may not be well-controlled.

5.5. Helmholtz inversion. This problem is motivated by anomalous behavior in a dielectric medium excited by a signal field [96]. Suppose we have a wave simulated by solving a Helmholtz equation with a point-disturbance located at θ ; our PDE is parameterized as

$$(5.4) \quad k^2(1 + \exp(-\frac{1}{2\alpha^2}\|\mathbf{x} - \theta\|_2^4))u(\mathbf{x}) + \nabla^2 u(\mathbf{x}) = 0, \quad \mathbf{x} \in \mathcal{X}$$

$$(5.5) \quad u(x, 0) = \cos(kx \cos(\gamma)), \quad u(0, y) = \cos(ky \sin(\gamma)),$$

$$(5.6) \quad u(1, y) = \cos(k(\cos(\gamma) + y \sin(\gamma))), \quad \frac{\partial u}{\partial y}(x, 1) \equiv 0$$

Here, we observe the PDE solution (with noise) at the two locations $(0.33, 1)$ and $(0.66, 1)$, e.g., we can only observe the behavior of the signal on the boundary of the domain. Further, we fix wave speed $k = 5$, wave angle $\gamma = \frac{\pi}{12}$, and anomaly concentration $2\alpha^2 = 10^{-4}$. The data were generated with parameter value $\theta^{\text{true}} = (0.3, 0.3)$. The solution to PDE (5.4) associated with θ^{true} is pictured in Figure 10. To show the efficacy of Algorithm 4.1 in conjunction with tempering, we consider only a single fidelity (i.e., $L = 0$) and use a small noise variance $\sigma^2 = 0.1 \times 2^{-6}$. The elliptic form of the PDE, small observational noise, and sparse observations make the posterior π have well-separated, nonlinear ridges with significant concentration. Results are reported in Table 4 and Figure 11.

This exercise demonstrates that tempering enables the surrogate (and its associated quadrature rule) to focus on regions of posterior concentration that traditional methods would not choose as evaluation points (cf. Figure 11, bottom left). While many compact-domain measure transport maps use bijections between $[0, 1]^d$ and \mathbb{R}^d and then perform approximation on \mathbb{R}^d [111], the concentration of this posterior near the boundary $\partial\Omega$ is particularly ill-suited to such approximations. In Section C we describe a class of transport maps \mathcal{F} that “natively” map from $[0, 1]^d$ to itself; this parameterization ensures that the ridges of high probability, shown in Figure 11, are adequately captured across the entire domain, especially near the domain boundaries.

These results also demonstrate that, while the posterior geometry is not obtained exactly, our algorithms work well in the single-fidelity setting, with 400 evaluations of the PDE solver. Table 5 compares the accuracy and cost of our final quadrature rule to the output of state-of-the-art SMC and interacting-chain MCMC algorithms [24, 42]. In this comparison, we interpret Q_M^{MIS} as an empirical

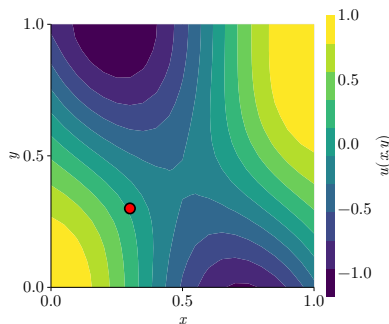
FIG. 10. True solution of PDE (5.4), where the red point is the location θ^{true} .

TABLE 4

Hyperparameters and error metrics for Subsection 5.5. Row j corresponds to Q_j^{MIS} and $\tilde{\pi}_j$. $n_j = 25$ at each step.

j	Hyperparameters		Error Metrics				
	β_j	p_j	rESS	RMSE	Förstner	MMD _G	MMD _{M_{1.5}}
0	0.075	14	8.10×10^{-1}	4.78×10^{-1}	5.38×10^{-1}	9.00×10^{-1}	9.04×10^{-1}
1	0.150	20	6.63×10^{-1}	4.71×10^{-1}	3.91×10^{-1}	7.77×10^{-1}	7.88×10^{-1}
2	0.300	20	5.37×10^{-1}	3.99×10^{-1}	3.00×10^{-1}	7.20×10^{-1}	7.34×10^{-1}
3	0.425	20	5.04×10^{-1}	3.12×10^{-1}	5.50×10^{-1}	7.07×10^{-1}	7.22×10^{-1}
4	0.450	27	5.00×10^{-1}	2.64×10^{-1}	4.78×10^{-1}	6.54×10^{-1}	6.70×10^{-1}
5	0.450	35	4.93×10^{-1}	3.32×10^{-1}	3.93×10^{-1}	6.41×10^{-1}	6.56×10^{-1}
6	0.500	44	5.01×10^{-1}	3.47×10^{-1}	3.85×10^{-1}	5.89×10^{-1}	6.00×10^{-1}
7	0.550	44	5.05×10^{-1}	5.42×10^{-1}	3.98×10^{-1}	6.13×10^{-1}	6.22×10^{-1}
8	0.625	54	5.04×10^{-1}	4.72×10^{-1}	3.50×10^{-1}	5.82×10^{-1}	5.91×10^{-1}
9	0.775	54	5.02×10^{-1}	5.18×10^{-1}	2.98×10^{-1}	5.55×10^{-1}	5.64×10^{-1}
10	0.825	65	5.02×10^{-1}	4.63×10^{-1}	2.80×10^{-1}	5.61×10^{-1}	5.69×10^{-1}
11	0.850	65	5.02×10^{-1}	5.87×10^{-1}	2.75×10^{-1}	5.69×10^{-1}	5.78×10^{-1}
12	0.875	65	5.00×10^{-1}	6.36×10^{-1}	2.81×10^{-1}	5.62×10^{-1}	5.69×10^{-1}
13	0.875	65	4.79×10^{-1}	6.85×10^{-1}	3.52×10^{-1}	5.65×10^{-1}	5.71×10^{-1}
14	1.000	77	5.03×10^{-1}	6.66×10^{-1}	3.08×10^{-1}	5.67×10^{-1}	5.73×10^{-1}
15	1.000	104	5.17×10^{-1}	6.41×10^{-1}	2.72×10^{-1}	5.75×10^{-1}	5.81×10^{-1}

measure, gather an equivalently sized quadrature rule from each of these alternative algorithms (requiring more than 400 likelihood evaluations), and compute the MMD between the empirical measures and π_M . See Section H for details. We find our Q_M^{MIS} yields smaller MMD at smaller cost.

We speculate that this performance could be improved further. The number of PDE evaluations was fixed arbitrarily, and the function class \mathcal{F}_j and other hyperparameters at step j were tuned in an ad hoc manner according to the a priori rESS diagnostic. We could also employ the multi-fidelity scheme, but the aim of this example is to highlight the standalone value of tempering and quadrature while comparing with related algorithms.

6. Conclusion. We have developed an iterative framework for the approximation and sampling of geometrically complex target distributions, based on a generalized annealing process, variational construction of transport maps, and the adaptive combination of importance-weighted quadrature rules. Our algorithms are suited to computationally expensive black-box models and can exploit a collection of forward models of varying fidelity. The aim of our framework is to *meet Bayesian practitioners where they are*: stranded without gradients and starved for model evaluations. Empirically, our generalized annealing scheme achieves good approximations of strongly non-Gaussian distributions with 100–400

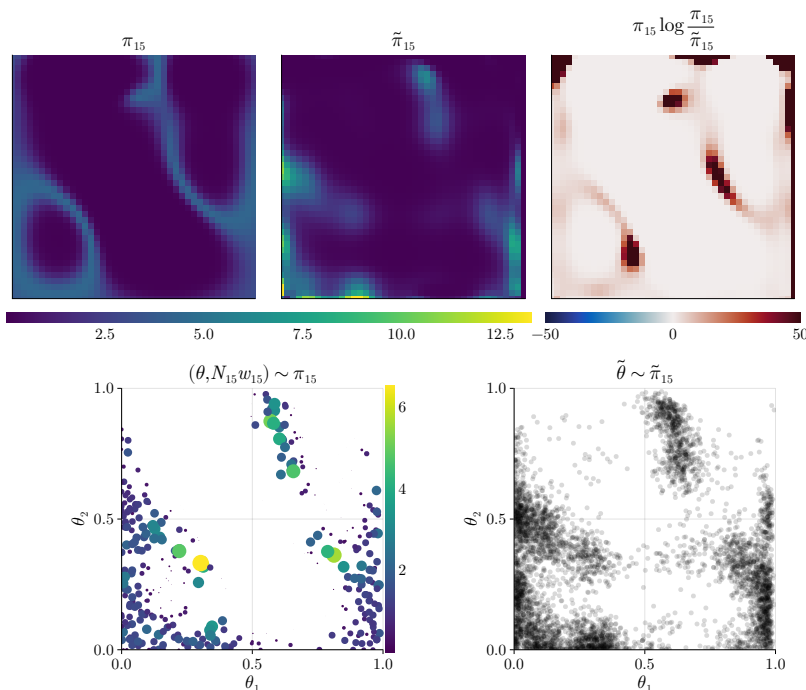


FIG. 11. Visualization of the results for Subsection 5.5. (Top): From left to right, we compare the truth, surrogate, and KL integrand. (Bottom left): Final quadrature Q_M^{MIS} . (Bottom right): Samples from the pullback distribution $\tilde{\pi}_M$.

TABLE 5
Other methods' performance approximating π_M in Subsection 5.5.

	# of likelihood evaluations	$\text{MMD}_{M_{1.5}}$	MMD_G
Q_M^{MIS}	400	0.580	0.610
SMC [24]	832	1.276	1.376
MCMC [42]	743	0.843	0.858

samples, while enjoying significant parallelizability—at a sample budget where a user of MCMC or SMC would still be awaiting convergence.

There are many important directions in which to expand and improve the present methods. First, our focus here has been on low-dimensional posterior distributions with expensive likelihoods and complex geometry. To extend the present approach to higher parameter dimensions, the modular structure of Algorithm 4.2 need not change significantly, but the transport maps and quadrature rules considered therein should be adapted to exploit more structure in the prior and posterior. For instance, it is known that triangular transport maps inherit sparse variable dependence [97] from conditional independence in the target [4, 93]. Similarly, many dimension reduction techniques for Bayesian inverse problems focus approximation and sampling on a low-dimensional subspace where the posterior departs most strongly from the prior. While many of these techniques are gradient-based [58, 109], recent methods [3] promise to identify such subspaces without gradient information and might be adapted here. In higher dimensions, the geometric tempering used here might induce Q_j with significantly lower rESS [14]. Thus, it is also of interest to consider other paths $(\pi_j)_j$, e.g., paths induced by Gaussian convolutions [110]. The design of “good” tempering paths, with notions of quality often quite specific to certain algorithms, is a very active area of research.

There is also a need for theory to characterize the convergence of our multiple importance-weighted quadrature schemes, given the cross-iteration dependencies and the use of structured quadrature rules (e.g., rQMC) as building blocks; this theory could yield sharper guidance on how to combine multiple rules, beyond the power heuristic and partition of unity used here. On this note, we find that several of our final rules Q_M^{MIS} contain quadrature points close in space with vastly different weights. Quantization [6] or kernel thinning [28] techniques could simplify these point sets to improve efficiency.

Acknowledgments. DS would like to thank Mathieu Le Provost for particularly illuminating discussions about compact-domain transport. DS and BvBW acknowledge support from the Laboratory Directed Research and Development program at Sandia National Laboratories, a multimission laboratory managed and operated by National Technology and Engineering Solutions of Sandia LLC, a wholly owned subsidiary of Honeywell International Inc., for the U.S. Department of Energy’s National Nuclear Security Administration under contract DE-NA0003525. DS and YMM also acknowledge support from the U.S. Department of Energy, Office of Science, Office of Advanced Scientific Computing Research, Scientific Discovery through Advanced Computing (SciDAC) Program through the FASTMath Institute, under contract number DE-AC52-07NA27344. DS also acknowledges support from a 2025–26 MathWorks Engineering Fellowship at MIT. SAND2026-18510R.

REFERENCES

- [1] M. S. ALBERGO AND E. VANDEN-ELJNDEN, *Learning to sample better*, Journal of Statistical Mechanics: Theory and Experiment, 2024 (2024), p. 104014.
- [2] C. ANDRIEU, N. CHOPIN, E. FINCATO, AND M. GERBER, *Gradient-free optimization via integration*, Aug. 2024.
- [3] R. BAPTISTA, M. BRENNAN, AND Y. MARZOUK, *Dimension reduction via score ratio matching*, Transactions on Machine Learning Research, (2025).
- [4] R. BAPTISTA, Y. MARZOUK, AND O. ZAHM, *On the Representation and Learning of Monotone Triangular Transport Maps*, Foundations of Computational Mathematics, (2023).
- [5] R. BAPTISTA, A. M. STUART, AND S. TRAN, *A Mathematical Perspective On Contrastive Learning*, May 2025.
- [6] A. BELHADJI, D. SHARP, AND Y. MARZOUK, *Weighted quantization using MMD: From mean field to mean shift via gradient flows*, May 2025.
- [7] D. BIGONI, A. SPANTINI, AND Y. MARZOUK, *Adaptive construction of measure transports for Bayesian inference.*, in NIPS Workshop on Approximate Inference, Jan. 2016.
- [8] D. M. BLEI, A. KUCUKELBIR, AND J. D. McAULIFFE, *Variational Inference: A Review for Statisticians*, Journal of the American Statistical Association, 112 (2017), pp. 859–877.
- [9] N. BONNOTTE, *From Knothe’s Rearrangement to Brenier’s Optimal Transport Map*, SIAM Journal on Mathematical Analysis, 45 (2013), pp. 64–87.
- [10] M. BRENNAN, D. BIGONI, O. ZAHM, A. SPANTINI, AND Y. MARZOUK, *Greedy inference with structure-exploiting lazy maps*, in Advances in Neural Information Processing Systems, vol. 33, 2020, pp. 8330–8342.
- [11] S. BROOKS, A. GELMAN, G. L. JONES, AND X. L. MENG, eds., *Handbook for Markov Chain Monte Carlo*, Taylor & Francis, 2011.
- [12] B. CALDERHEAD, *A general construction for parallelizing Metropolis-Hastings algorithms*, Proceedings of the National Academy of Sciences, 111 (2014), pp. 17408–17413.
- [13] F. CÉROU, P. HÉAS, AND M. ROUSSET, *Adaptive reduced tempering for Bayesian inverse problems and rare event simulation*, SIAM/ASA Journal on Uncertainty Quantification, 13 (2025), pp. 2022–2053.
- [14] O. CHEHAB, A. KORBA, A. J. STROMME, AND A. VACHER, *Provable convergence and limitations of geometric tempering for Langevin dynamics*, in Thirteenth International Conference on Learning Representations, 2025.
- [15] N. CHOPIN, F. R. CRUCINIO, AND A. KORBA, *A connection between Tempering and Entropic Mirror Descent*, June 2024.
- [16] N. CHOPIN AND O. PAPASPILIOPOULOS, *An Introduction to Sequential Monte Carlo*, Springer Series in Statistics, Springer International Publishing, 2020.
- [17] J. A. CHRISTEN AND C. FOX, *Markov chain Monte Carlo Using an Approximation*, Journal of Computational and Graphical Statistics, 14 (2005), pp. 795–810.
- [18] P. R. CONRAD, A. D. DAVIS, Y. MARZOUK, N. S. PILLAI, AND A. SMITH, *Parallel Local Approximation MCMC for Expensive Models*, SIAM/ASA Journal on Uncertainty Quantification, 6 (2018), pp. 339–373.
- [19] P. R. CONRAD AND Y. MARZOUK, *Adaptive Smolyak Pseudospectral Approximations*, SIAM Journal on Scientific Computing, 35 (2013), pp. A2643–A2670.
- [20] P. R. CONRAD, Y. MARZOUK, N. S. PILLAI, AND A. SMITH, *Accelerating Asymptotically Exact MCMC for Computationally Intensive Models via Local Approximations*, Journal of the American Statistical Association, 111 (2016), pp. 1591–1607.
- [21] T. CUI AND S. DOLGOV, *Deep Composition of Tensor-Trains Using Squared Inverse Rosenblatt Transports*,

- Foundations of Computational Mathematics, 22 (2022), pp. 1863–1922.
- [22] T. CUI, S. DOLGOV, AND R. SCHEICHL, *Deep Importance Sampling Using Tensor Trains with Application to a Priori and a Posteriori Rare Events*, SIAM Journal on Scientific Computing, 46 (2024), pp. C1–C29.
- [23] T. CUI, S. DOLGOV, AND O. ZAHM, *Scalable conditional deep inverse Rosenblatt transports using tensor trains and gradient-based dimension reduction*, Journal of Computational Physics, 485 (2023), p. 112103.
- [24] H.-D. DAU AND N. CHOPIN, *Waste-Free Sequential Monte Carlo*, Journal of the Royal Statistical Society Series B: Statistical Methodology, 84 (2022), pp. 114–148.
- [25] A. D. DAVIS, Y. MARZOUK, A. SMITH, AND N. PILLAI, *Rate-optimal refinement strategies for local approximation MCMC*, Statistics and Computing, 32 (2022), p. 60.
- [26] L. DEVROYE, *Non-Uniform Random Variate Generation*, Springer New York, 1986.
- [27] S. DOLGOV, K. ANAYA-IZQUIERDO, C. FOX, AND R. SCHEICHL, *Approximation and sampling of multivariate probability distributions in the tensor train decomposition*, Statistics and Computing, 30 (2020), pp. 603–625.
- [28] R. DWIVEDI AND L. MACKEY, *Kernel thinning*, Journal of Machine Learning Research, 25 (2024), pp. 1–77.
- [29] S. ECKSTEIN AND G. PAMMER, *Computational methods for adapted optimal transport*, The Annals of Applied Probability, 34 (2024).
- [30] T. A. EL MOSELHY AND Y. MARZOUK, *Bayesian inference with optimal maps*, Journal of Computational Physics, 231 (2012), pp. 7815–7850.
- [31] M. EL DRED, *Recent Advances in Non-Intrusive Polynomial Chaos and Stochastic Collocation Methods for Uncertainty Analysis and Design*, in 50th AIAA/ASME/ASCE/AHS/ASC Structures, Structural Dynamics, and Materials Conference, American Institute of Aeronautics and Astronautics, May 2009.
- [32] O. G. ERNST, H. GOTTSCHALK, T. KOWALEWITZ, AND P. KRÜGER, *Learning to Integrate*, June 2025.
- [33] I.-G. FARCAS, J. LATZ, E. ULLMANN, T. NECKEL, AND H.-J. BUNGARTZ, *Multilevel adaptive sparse Leja approximations for Bayesian inverse problems*, SIAM Journal on Scientific Computing, 42 (2020), pp. A424–A451.
- [34] L. FELARDOS, J. HÉNIN, AND G. CHARPIAT, *Designing losses for data-free training of normalizing flows on Boltzmann distributions*, Jan. 2023.
- [35] J. FEYDY, T. SÉJOURNÉ, F.-X. VIALARD, S.-I. AMARI, A. TROUVE, AND G. PEYRÉ, *Interpolating between Optimal Transport and MMD using Sinkhorn Divergences*, in Proceedings of the Twenty-Second International Conference on Artificial Intelligence and Statistics, PMLR, Apr. 2019, pp. 2681–2690.
- [36] W. FÖRSTNER AND B. MOONEN, *A Metric for Covariance Matrices*, in Geodesy - The Challenge of the 3rd Millennium, Springer, 2003, pp. 299–309.
- [37] M. GABRIÉ, G. M. ROTSKOFF, AND E. VANDEN-EIJNDEN, *Adaptive Monte Carlo augmented with normalizing flows*, Proceedings of the National Academy of Sciences, 119 (2022), p. e2109420119.
- [38] M. J. GANDER AND A. H. KARP, *Stable computation of high order Gauss quadrature rules using discretization for measures in radiation transfer*, Journal of Quantitative Spectroscopy and Radiative Transfer, 68 (2001), pp. 213–223.
- [39] A. GARBUNO-INIGO, F. HOFFMANN, W. LI, AND A. M. STUART, *Interacting Langevin Diffusions: Gradient Structure and Ensemble Kalman Sampler*, SIAM Journal on Applied Dynamical Systems, 19 (2020), pp. 412–441.
- [40] W. GAUTSCHI, *Algorithm 726: ORTHPOL—a package of routines for generating orthogonal polynomials and Gauss-type quadrature rules*, ACM Transactions on Mathematical Software (TOMS), 20 (1994), pp. 21–62.
- [41] C. J. GEYER AND E. A. THOMPSON, *Annealing Markov Chain Monte Carlo with Applications to Ancestral Inference*, Journal of the American Statistical Association, (1995).
- [42] J. GOODMAN AND J. WEARE, *Ensemble samplers with affine invariance*, Communications in Applied Mathematics and Computational Science, 5 (2010), pp. 65–80.
- [43] H. HAARIO, E. SAKSMAN, AND J. TAMMINEN, *An adaptive Metropolis algorithm*, Bernoulli, 7 (2001), pp. 223–242.
- [44] T. HESTERBERG, *Weighted average importance sampling and defensive mixture distributions*, Technometrics : a journal of statistics for the physical, chemical, and engineering sciences, 37 (1995), pp. 185–194.
- [45] D. HIGDON, H. LEE, AND ZHUOXIN BI, *A Bayesian approach to characterizing uncertainty in inverse problems using coarse and fine-scale information*, IEEE Transactions on Signal Processing, 50 (2002), pp. 389–399.
- [46] B. HOSSEINI, A. W. HSU, AND A. TAGHVAEI, *Conditional Optimal Transport on Function Spaces*, Feb. 2024.
- [47] P. E. JACOB, J. O’LEARY, AND Y. F. ATCHADÉ, *Unbiased Markov Chain Monte Carlo Methods with Couplings*, Journal of the Royal Statistical Society Series B: Statistical Methodology, 82 (2020), pp. 543–600.
- [48] J. JAKEMAN, F. FRANZELIN, A. NARAYAN, M. EL DRED, AND D. PFLÜGER, *Polynomial chaos expansions for dependent random variables*, Computer Methods in Applied Mechanics and Engineering, 351 (2019), pp. 643–666.
- [49] G. JERFEL, S. WANG, C. WONG-FANNJIANG, K. A. HELLER, Y. MA, AND M. I. JORDAN, *Variational refinement for importance sampling using the forward Kullback-Leibler divergence*, in Proceedings of the Thirty-Seventh Conference on Uncertainty in Artificial Intelligence, PMLR, Dec. 2021, pp. 1819–1829.
- [50] J. KAIPIO AND E. SOMERSALO, *Statistical inverse problems: Discretization, model reduction and inverse crimes*, Journal of Computational and Applied Mathematics, 198 (2007), pp. 493–504.
- [51] A. KATSEVICH AND P. RIGOLLET, *On the approximation accuracy of Gaussian variational inference*, The Annals of Statistics, 52 (2024).
- [52] D. KIM, K. SONG, S. SHIN, W. KANG, I.-C. MOON, AND W. JOO, *Sequential Neural Joint Estimation for likelihood-free inference*, Journal of the Korean Statistical Society, (2025).

- [53] I. KLEBANOV AND T. J. SULLIVAN, *Transporting Higher-Order Quadrature Rules: Quasi-Monte Carlo Points and Sparse Grids for Mixture Distributions*, Aug. 2023.
- [54] H. KNOTHE, *Contributions to the theory of convex bodies.*, Michigan Mathematical Journal, 4 (1957).
- [55] D. P. KROESE, R. Y. RUBINSTEIN, AND P. W. GLYNN, *The Cross-Entropy Method for Estimation*, in Handbook of Statistics, vol. 31, Elsevier, 2013, pp. 19–34.
- [56] M. LAMBERT, S. CHEWI, F. BACH, S. BONNABEL, AND P. RIGOLLET, *Variational inference via Wasserstein gradient flows*, in Advances in neural information processing systems, vol. 35, 2022, pp. 14434–14447.
- [57] J. LI AND Y. MARZOUK, *Adaptive Construction of Surrogates for the Bayesian Solution of Inverse Problems*, SIAM Journal on Scientific Computing, 36 (2014), pp. A1163–A1186.
- [58] M. LI, T. CUI, F. LI, Y. MARZOUK, AND O. ZAHM, *Sharp detection of low-dimensional structure in probability measures via dimensional logarithmic Sobolev inequalities*, Information and Inference, 14 (2025).
- [59] B. LIU, *Adaptive annealed importance sampling for multimodal posterior exploration and model selection with application to extrasolar planet detection*, The Astrophysical Journal Supplement Series, 213 (2014), p. 14.
- [60] S. LIU, *Transport Quasi-Monte Carlo*, Dec. 2024.
- [61] F. LU, M. MORZFELD, X. TU, AND A. J. CHORIN, *Limitations of polynomial chaos expansions in the Bayesian solution of inverse problems*, Journal of Computational Physics, 282 (2015), pp. 138–147.
- [62] J. MA, V. ROKHLIN, AND S. WANDZURA, *Generalized Gaussian quadrature rules for systems of arbitrary functions*, SIAM Journal on Numerical Analysis, 33 (1996), pp. 971–996.
- [63] J. MARTIN, L. C. WILCOX, C. BURSTEDDE, AND O. GHATTAS, *A Stochastic Newton MCMC Method for Large-Scale Statistical Inverse Problems with Application to Seismic Inversion*, SIAM Journal on Scientific Computing, 34 (2012), pp. A1460–A1487.
- [64] Y. MARZOUK, T. MOSELHY, M. PARNO, AND A. SPANTINI, *Sampling via Measure Transport: An Introduction*, in Handbook of Uncertainty Quantification, Springer International Publishing, 2016, pp. 1–41.
- [65] Y. MARZOUK AND H. N. NAJM, *Dimensionality reduction and polynomial chaos acceleration of Bayesian inference in inverse problems*, Journal of Computational Physics, 228 (2009), pp. 1862–1902.
- [66] Y. MARZOUK, H. N. NAJM, AND L. A. RAHN, *Stochastic spectral methods for efficient Bayesian solution of inverse problems*, Journal of Computational Physics, 224 (2007), pp. 560–586.
- [67] Y. MARZOUK AND D. XIU, *A stochastic collocation approach to Bayesian inference in inverse problems*, Communications in Computational Physics, 6 (2009), pp. 826–847.
- [68] A. MAURAS AND Y. MARZOUK, *Sampling in Unit Time with Kernel Fisher-Rao Flow*, in Proceedings of the 41st International Conference on Machine Learning, vol. 235, PMLR, July 2024, pp. 35138–35162.
- [69] N. METROPOLIS, A. W. ROSENBLUTH, M. N. ROSENBLUTH, A. H. TELLER, AND E. TELLER, *Equation of State Calculations by Fast Computing Machines*, The Journal of Chemical Physics, 21 (1953), pp. 1087–1092.
- [70] L. I. MIDGLEY, V. STIMPER, G. N. C. SIMM, B. SCHÖLKOPF, AND J. M. HERNÁNDEZ-LOBATO, *Flow Annealed Importance Sampling Bootstrap*, Mar. 2023.
- [71] K. MUANDET, K. FUKUMIZU, B. SRIPERUMBUDUR, B. SCHÖLKOPF, ET AL., *Kernel mean embedding of distributions: A review and beyond*, Foundations and Trends® in Machine Learning, 10 (2017), pp. 1–141.
- [72] T. MÜLLER, B. MCWILLIAMS, F. ROUSSELLE, M. GROSS, AND J. NOVÁK, *Neural Importance Sampling*, ACM Transactions on Graphics, 38 (2019), pp. 1–19.
- [73] C. NAESSETH, F. LINDSTEN, AND D. BLEI, *Markovian Score Climbing: Variational Inference with $KL(p||q)$* , in Advances in Neural Information Processing Systems, vol. 33, 2020, pp. 15499–15510.
- [74] W. NEISWANGER, C. WANG, AND E. XING, *Asymptotically Exact, Embarrassingly Parallel MCMC*, Mar. 2014.
- [75] A. OLIVIER, D. G. GIOVANIS, B. AAKASH, M. CHAUHAN, L. VANDANAPU, AND M. D. SHIELDS, *UQpy: A general purpose Python package and development environment for uncertainty quantification*, Journal of Computational Science, 47 (2020), p. 101204, <https://doi.org/10.1016/j.jocs.2020.101204>.
- [76] A. OWEN AND Y. ZHOU, *Safe and effective importance sampling*, Journal of the American Statistical Association, 95 (2000), pp. 135–143.
- [77] A. B. OWEN, *Randomly Permuted (t,m,s) -Nets and (t, s) -Sequences*, in Monte Carlo and Quasi-Monte Carlo Methods in Scientific Computing, H. Niederreiter and P. J.-S. Shiue, eds., Springer, 1995, pp. 299–317.
- [78] A. B. OWEN, *Monte Carlo Theory, Methods and Examples*, <https://artowen.su.domains/mc/>, 2013.
- [79] M. PARNO, P.-B. RUBIO, D. SHARP, M. BRENNAN, R. BAPTISTA, H. BONART, AND Y. MARZOUK, *MParT: Monotone Parameterization Toolkit*, Journal of Open Source Software, 7 (2022), p. 4843, <https://doi.org/10.21105/joss.04843>.
- [80] M. D. PARNO AND Y. MARZOUK, *Transport Map Accelerated Markov Chain Monte Carlo*, SIAM/ASA Journal on Uncertainty Quantification, 6 (2018), pp. 645–682.
- [81] B. PEHERSTORFER, T. CUI, Y. MARZOUK, AND K. WILLCOX, *Multifidelity importance sampling*, Computer Methods in Applied Mechanics and Engineering, 300 (2016), pp. 490–509.
- [82] B. PEHERSTORFER, K. WILLCOX, AND M. GUNZBURGER, *Survey of Multifidelity Methods in Uncertainty Propagation, Inference, and Optimization*, SIAM Review, 60 (2018), pp. 550–591.
- [83] M. RAMGRABER, D. SHARP, M. LE PROVOST, AND Y. MARZOUK, *A friendly introduction to triangular transport*, Mar. 2025.
- [84] R. RANGANATH, S. GERRISH, AND D. BLEI, *Black box variational inference*, in Proceedings of the seventeenth international conference on artificial intelligence and statistics, vol. 33, PMLR, Apr. 2014, pp. 814–822.
- [85] D. REZENDE AND S. MOHAMED, *Variational inference with normalizing flows*, in International Conference on Machine Learning, PMLR, 2015, pp. 1530–1538.

- [86] C. P. ROBERT AND G. CASELLA, *Monte Carlo Statistical Methods*, Springer Texts in Statistics, Springer New York, 2004.
- [87] M. ROSENBLATT, *Remarks on a Multivariate Transformation*, The Annals of Mathematical Statistics, 23 (1952), pp. 470–472.
- [88] R. RUBINSTEIN, *The Cross-Entropy Method for Combinatorial and Continuous Optimization*, Methodology And Computing In Applied Probability, 1 (1999), pp. 127–190.
- [89] B. SALEH, A. ZIMMERMAN, P. CHEN, AND O. GHATTAS, *Tempered multifidelity importance sampling for gravitational wave parameter estimation*, Physical Review D, 110 (2024), p. 104037.
- [90] K. SARGSYAN, B. DEBUSSCHERE, H. NAJM, AND O. L. MAÏTRE, *Spectral Representation and Reduced Order Modeling of the Dynamics of Stochastic Reaction Networks via Adaptive Data Partitioning*, SIAM Journal on Scientific Computing, 31 (2010), pp. 4395–4421.
- [91] I. M. SOBOLOV, *On the distribution of points in a cube and the approximate evaluation of integrals*, USSR Computational Mathematics and Mathematical Physics, 7 (1967), pp. 86–112.
- [92] D. A. D. SOUZA, D. MESQUITA, S. KASKI, AND L. ACERBI, *Parallel MCMC Without Embarrassing Failures*, in Proceedings of The 25th International Conference on Artificial Intelligence and Statistics, PMLR, May 2022, pp. 1786–1804.
- [93] A. SPANTINI, D. BIGONI, AND Y. MARZOUK, *Inference via low-dimensional couplings*, Journal of Machine Learning Research, 19 (2018), pp. 1–71.
- [94] A. H. STROUD, *Approximate Calculation of Multiple Integrals*, Prentice-Hall, 1971.
- [95] S. SYED, A. BOUCHARD-CÔTÉ, K. CHERN, AND A. DOUCET, *Optimised Annealed Sequential Monte Carlo Samplers*, Aug. 2024.
- [96] M. TADI, A. NANDAKUMARAN, AND S. SRITHARAN, *An inverse problem for Helmholtz equation*, Inverse Problems in Science and Engineering, 19 (2011), pp. 839–854.
- [97] X. T. TONG, M. MORZFELD, AND Y. M. MARZOUK, *MALA-within-Gibbs Samplers for High-Dimensional Distributions with Sparse Conditional Structure*, SIAM Journal on Scientific Computing, 42 (2020), pp. A1765–A1788.
- [98] VARIOUS CONTRIBUTORS, *SciML/QuasiMonteCarlo.jl*. SciML Open Source Scientific Machine Learning, 2019.
- [99] VARIOUS CONTRIBUTORS, *FluxML/Optimisers.jl*. FluxML, 2022.
- [100] E. VEACH, *Robust Monte Carlo Methods for Light Transport Simulation*, PhD thesis, Stanford University, 1998.
- [101] C. VILLANI, *Optimal Transport: Old and New*, vol. 338, Springer, 2009.
- [102] L. WANG AND N. NÜSKEN, *Measure transport with kernel mean embeddings*, arXiv preprint, (2024).
- [103] S. WANG AND Y. MARZOUK, *On minimax density estimation via measure transport*, Sept. 2022.
- [104] Y. WANG, C. CHI, AND A. R. DINNER, *Mitigating mode collapse in normalizing flows by annealing with an adaptive schedule: Application to parameter estimation*, May 2025.
- [105] Z. O. WANG, R. BAPTISTA, Y. MARZOUK, L. RUTHOTTO, AND D. VERMA, *Efficient Neural Network Approaches for Conditional Optimal Transport with Applications in Bayesian Inference*, July 2024.
- [106] T. WILDEY, B. VAN BLOEMEN WAANDERS, D. RIDZAL, D. SEIDL, G. HARPER, AND B. REUTER, *MrHyDE v.1.0*, tech. report, Sandia National Lab. (SNL-NM), Albuquerque, NM (United States), Oct. 2023.
- [107] D. XIU AND G. E. KARNIADAKIS, *The Wiener–Askey Polynomial Chaos for Stochastic Differential Equations*, SIAM Journal on Scientific Computing, 24 (2002), pp. 619–644.
- [108] L. YAN AND T. ZHOU, *Adaptive multi-fidelity polynomial chaos approach to Bayesian inference in inverse problems*, Journal of Computational Physics, 381 (2019), pp. 110–128.
- [109] O. ZAHM, T. CUI, K. LAW, A. SPANTINI, AND Y. MARZOUK, *Certified dimension reduction in nonlinear Bayesian inverse problems*, Mathematics of Computation, 91 (2022), pp. 1789–1835.
- [110] B. ZANGER, T. CUI, M. SCHREIBER, AND O. ZAHM, *Sequential transport maps using SoS density estimation and α -divergences*, Feb. 2024.
- [111] L. ZENG, X. WAN, AND T. ZHOU, *Bounded KRnet and Its Applications to Density Estimation and Approximation*, SIAM Journal on Scientific Computing, 47 (2025), pp. C1294–C1318.
- [112] J. ZHANG AND A. A. TAFLANIDIS, *Accelerating MCMC via Kriging-based adaptive independent proposals and delayed rejection*, Computer Methods in Applied Mechanics and Engineering, 355 (2019), pp. 1124–1147.

Appendix A. Integral discretization details. Since we assume uniform prior $\pi_\theta = U(0, 1)^d$, we use randomized QMC methods. More specifically, given a dimension d and desired quadrature evaluations n , we find the smallest prime base $b \in \mathbb{N}$ such that $b > d$ and smallest padding $p \in \mathbb{N}$ such that $b^p > n$. Then, we take n of the first b^p points from a scrambled, d -dimensional QMC sequence. In Section 5, we use the Sobol’ sequence [91] and employ Owen’s scramble [77], both implemented in [98].

Appendix B. Adaptive selection of tempering parameter. We briefly summarize an adaptive method inspired by [57, 104], adjusted for our use-case, to choose tempering parameter β adaptively. Recall the definition of the relative effective sample size rESS for a normalized set of weights $(w^{(k)})_{k=1}^N \subset [0, 1]$ as $\text{rESS}[\mathbf{w}] = (N \|\mathbf{w}\|_2^2)^{-1}$. Then, we fix a global discount parameter ρ and minimum rESS value $r_{\min} \in (0, 1)$. We choose $\rho = 0.8$ and $r_{\min} = 0.5$ and create a monotone sequence of tempering candidates $\mathcal{B} = (b_q)_{q=1}^{N_\beta} \subset (0, 1)$, chosen as $b_q = q/N_\beta$ for $N_\beta = 40$ in Section 5. Then,

our procedure to choose β_{j+1} is given in Algorithm B.1.

Algorithm B.1 Adaptively choosing tempering parameter

Input: Tempering candidates \mathcal{B} , discount $\rho \in (0, 1)$, previous rESS value r_j , previous tempering β_j , rESS floor $r_{\min} \in (0, 1)$, and Algorithm 4.1 arguments $A = (\tilde{\pi}_{i-1}, D_i)_{i=j_0}^j$
Output: Tempering parameter β_{j+1} , quadrature rule Q_{j+1} , and rESS r_{j+1}
set index $q = N_\beta$ and $r_{\min} = \max(\rho r_j, r_{\min})$
while $q > 0$ and $r_q > r_{\min}$ and $b_q \leq \beta_j$ **do**
 Create quadrature rule P_q from **Algorithm 4.1** with tempering $\beta = b_q$ and arguments A .
 set $r_q = \text{rESS}[P_q]$ then decrement q .
end while
set $\beta_{j+1} = b_{q+1}$, $Q_{j+1} = P_{q+1}$, and $r_{j+1} = \text{rESS}[P_{q+1}]$

We use Algorithm B.1 *in place* of Algorithm 4.1 inside of Algorithm 4.2. In future work, we propose varying minimum threshold r_{\min} as β_j increases; while Algorithm B.1 allows for some flexibility above r_{\min} , we may want to increase threshold r_{\min} as $j \rightarrow M$, i.e., as $\beta_j \rightarrow 1$.

Appendix C. Parameterizing transport maps on the unit hypercube. The Knothe–Rosenblatt rearrangement (often also called KR map or triangular transport map) is a popular measure transport method [4, 54, 80, 87, 101], which in one-dimension is exactly the “inverse-CDF trick” [26]: if we have $Z \sim \eta = U(0, 1)$ and a target density $\pi \in \mathcal{C}^1$ with cumulative distribution function (CDF) $F_\pi : \mathbb{R} \rightarrow [0, 1]$, we know that F_π is invertible and $F_\pi^{-1}(Z) \sim \pi$. We thus have identity $F_{\pi\#}\pi = \eta$ and its converse $F_\pi\#\eta = \pi$. For the uniform reference case, i.e., when $\eta = U(0, 1)^d$, the KR map is an extension of the above by factoring the joint density into its conditionals:

$$\pi(\theta_1, \theta_2, \dots, \theta_d) = \pi^{(1)}(\theta_1) \pi^{(2)}(\theta_2|\theta_1) \pi^{(3)}(\theta_3|\theta_1, \theta_2) \dots \pi^{(d)}(\theta_d|\theta_1, \dots, \theta_{d-1}).$$

Given $Z_1, \dots, Z_d \sim U(0, 1)$, we set $\theta_1 = F_{\pi^{(1)}}^{-1}(Z_1)$ and know $\theta_1 \sim \pi^{(1)}$. Conditioned on this fixed θ_1 , univariate density $\pi^{(2)}$ has CDF $F_{\pi^{(2)}}(\theta_2; \theta_1) = \int_0^{\theta_2} d\pi^{(2)}(t|\theta_1) dt$, so $\theta_2 = F_{\pi^{(2)}}(\cdot; \theta_1)^{-1}(Z_2) \sim \pi^{(2)}(\theta_2|\theta_1)$; this continues for $j = 3, \dots, d$ via

$$(C.1) \quad \theta_j = F_{\pi^{(j)}}^{-1}(\cdot; \theta_1, \dots, \theta_{j-1})(Z_j), \quad F_{\pi^{(j)}}(\theta_j; \theta_1, \dots, \theta_{j-1}) = \int_0^{\theta_j} \pi^{(j)}(t | \theta_1, \dots, \theta_{j-1}) dt.$$

This transport map construction has earned the “triangular transport” moniker since the map $S = (F_{\pi^{(1)}}, F_{\pi^{(2)}}, \dots, F_{\pi^{(d)}})$ has a lower-triangular Jacobian matrix, an artifact of its conditional CDF construction, meaning that the pullback density $\pi(\theta) = \eta(S(\theta))|\nabla S(\theta)|$ is simple to calculate. There are many approximations of KR maps in literature, e.g., [23, 29, 90, 105, 110]. We choose a parametric approximation from [103], which has interesting theoretical results but no prior implementation, though it is heavily inspired work in, e.g., [4, 64, 80]. Using reference $\eta = U(0, 1)^d$ and recalling the conditional CDF structure of S from (C.1), a natural characterization of $S^{(d)}$ is to then create a *positive-valued* parametric function $f_d(\cdot, \cdot; c_d) : [0, 1]^{d-1} \times [0, 1] \times \mathbb{R}^{p_d} \rightarrow \mathbb{R}^+$, parameterized by some $c_d \in \mathbb{R}^{p_d}$, and use f_d to proportionally approximate $\pi^{(d)}(t|\theta_{1:d-1}) \propto f_d(\theta_{1:d-1}, t; c_d)$. Then,

$$I_d(s; \theta_{1:d-1}, c_d) := \int_0^s f_d(\theta_{1:d-1}, t; c_d) dt, \quad S^{(d)}(\theta; c_d) := \frac{I_d(\theta_d; \theta_{1:d-1}, c_d)}{I_d(1; \theta_{1:d-1}, c_d)}.$$

Since $f_d \approx \pi^{(d)}$ is an unnormalized conditional density, the denominator ensures $S^{(d)}(\theta_{1:d-1}, 1) \equiv 1$. Therefore, we calculate the CDF of the conditional distribution $\pi^{(d)}$ by employing its unnormalized approximation and then normalizing it. Notably, both integrals in this expression are one-dimensional and thus tractable using traditional quadrature techniques. We do not vary inputs $\theta_{1:d-1}$ or c_d while calculating I_d , indicating that the parameterization of f_d dictates the expense to evaluate I_d . We

choose to use $f_d(\theta_{1:d-1}, t; c_d) = r(g_M(\theta_{1:d-1}, t)^\top c_d)$, where rectifier $r : \mathbb{R} \rightarrow \mathbb{R}^+$ is a positive, monotone increasing function, and $g_M : \mathbb{R}^d \rightarrow \mathbb{R}^{p_d}$ is an arbitrary set of basis functions. In this paper, we use rectifier $r(t) = \log(1 + \exp(t))$ and g_M as a total order M set of tensor-product shifted Legendre polynomials. Each output of g_M is thus a product of univariate shifted Legendre polynomials and has at most $M + 1$ nonzero mixed derivatives, i.e., for all $a \in [p_j]$, we know $\frac{\partial^{\vec{a}}}{\partial \theta^{\vec{a}}} g_a = 0$ when multi-index \vec{a} satisfies $\|\vec{a}\|_1 > M$. For more on triangular transport with details on our implementation and optimization, see Section E. Further, see [4, 7, 64] for computation and [83] for a tutorial.

Appendix D. Example of multiple importance sampling. We use a toy set of parameters to illuminate the complex connections of multiple IS, particularly with a focus on the cumulative integration technique proposed in Algorithm 4.1. Suppose there is a point θ_0^* such that $\pi_\theta(\theta_0^*) = 0.25$ but $\tilde{\pi}_1(\theta_0^*) = 0.75$ with $n_0 = 2n_1$. Then,

$$\alpha_0(\theta_0^*) = \frac{(n_0 \pi_\theta(\theta_0^*))^2}{(n_0 \pi_\theta(\theta_0^*))^2 + (n_1 \tilde{\pi}_0(\theta_0^*))^2} = \frac{(0.25)^2}{(0.25)^2 + (1.5)^2} \approx 0.027,$$

exemplifying that, if $\hat{\pi}_j \ll \hat{\pi}_{j'}$ at $\theta_j^{(k)}$, then $\alpha_j(\theta_j^{(k)})$ will be very small. On the other hand, if the two biasing distributions give similar values, the integral is split more equally between the biasing distributions near $\theta_j^{(k)}$.

Appendix E. Further discussion for transport maps. Below, we include a few supplemental remarks detailing the relationship of triangular maps used in this paper to optimal transport, often important for readers unfamiliar with statistical transport map techniques. We also include details of the parameterization, which is largely an extension of discussions in [83], and add a few implementation notes vital for reproducing results.

E.1. Relating KR maps and Optimal Transport. While the one-dimensional case boils down to the exact same solution as one would get performing *optimal transport*, the KR map generally will not coincide with the “optimal” map as the reader may see discussed in, e.g., [35, 101]; instead, it reflects some sense of “conditional optimality” because of the sequence of conditional CDF transports [9, 46, 105]. Regardless, the lack of optimality will not change the algorithm nor will it disrupt the practicality, for we only seek to couple π and η via some map S . We have no need for S to perform minimal work so long as it takes us between π and η in an invertible fashion, and the triangular map gives a computationally convenient methodology for doing so (much more so than most optimal transport methods).

E.2. Details of polynomial expansions. Consider a set of univariate bases $\{\psi_k^{(d)}\}_{d,k}$, with $\psi_k^{(d)}$ as the k th univariate basis function for input dimension d . For example, consider a two-dimensional problem with $\psi_k^{(1)}(\theta) = \sin(2\pi k\theta)$ and $\psi_k^{(2)}$ as the k 'th Legendre polynomial \tilde{p}_k . These are both orthogonal sets on $L_2([0, 1])$. Similar to multivariate polynomial surrogate construction [19, 48, 107], we choose a set of multi-indices $\mathcal{A} \subset \mathbb{N}_0^d$ to describe the function class for f_d ; in all examples, we choose *total order* sets $\mathcal{A}_T^d := \{\vec{\alpha} \in \mathbb{N}_0^d \mid \|\vec{\alpha}\|_1 \leq T\}$. We understand $\vec{\alpha}$ as representing a *multivariate basis function* $\Psi_{\vec{\alpha}}(\theta) = \prod_{j=1}^d \psi_{\alpha_j}^{(j)}(\theta_j)$. This inundates the reader with notation, but returning to the prior example, multi-index $\vec{\alpha} = (2, 1)$ produces multivariate basis function $\Psi_{(2,1)} = \sin(4\pi\theta_1)\tilde{p}_1(\theta_2)$. We then create an expansion $\hat{f}_d(\theta; c_d) = \sum_{\vec{\alpha} \in \mathcal{A}} c_{\vec{\alpha}} \Psi_{\vec{\alpha}}$. Further, to satisfy the positivity constraint $f_d > 0$, we choose a *rectifier* $r : \mathbb{R} \rightarrow \mathbb{R}^+$ (e.g., $r(s) = \exp(s)$ or $r(s) = \log(1 + \exp(s))$). Finally, we set $f_d(\theta_{1:d}; c_d) = r(\partial_d \hat{f}_d(\theta_{1:d}; c_d))$. The intuition here in the scalar case is that, for rectifier $r(s) = \exp(s)$ and reference density $\eta = U(0, 1)$, we get $\log S^\# \eta = \log \eta \circ S + \log \partial_\theta S = \hat{f}(\theta; c) - \log \int_0^1 \exp(\hat{f}(t; c)) dt$, so we explicitly perform parametric density estimation via $\hat{f} \approx \log \pi + C$

E.3. Optimization and hyperparameters. All approximation for the transport maps in Section 5 are shifted Legendre polynomials with the softplus rectifier and adaptive Clenshaw-Curtis quadrature as implemented in [79]. For optimizing S , we use 10^3 Nesterov optimization steps

(with default hyperparameters of $\eta = 0.001, \rho = 0.9$) of size 10^{-3} as implemented in [99], with L_2 regularization of size 10^{-3} . For total order maps, we have $p_d = \text{nCr}(M + d, d)$ with binomial coefficient nCr . Table 6 thus describes the total order used for each example in Section 5.

TABLE 6

Total order of transport maps for each step of examples. Bold indicates the first step for a given likelihood fidelity.

Example	j															
	0	1	2	3	4	5	6	7	8	9	10	11	12	13	14	15
Single source diffusion	4	4	5	5	3	3	7									
Multiple source diffusion	4	6	6	3	3	6	7									
Convection diffusion reaction	3	5	4	5	3	5	7	7	7							
Helmholtz	4	5	5	5	6	7	8	8	9	9	10	10	11	12	12	13

Appendix F. Error metric background and details. First, given a symmetric-positive kernel function $K : \mathbb{R}^d \times \mathbb{R}^d \rightarrow \mathbb{R}^+$ (i.e., $K(x, y) = K(y, x) \geq 0$), we define the MMD as

$$\text{MMD}_K^2(\pi, \tilde{\pi}) = \mathbb{E}_{\pi, \pi}[K(X, X')] - 2\mathbb{E}_{\pi, \tilde{\pi}}[K(X, Y)] + \mathbb{E}_{\tilde{\pi}, \tilde{\pi}}[K(Y, Y')].$$

We use two distance-based kernels: squared-exponential and Matèrn-1.5, denoted $K_S(x, y) = k_S(\|x - y\|_2 / \sigma_{\text{MMD}})$ and $K_{M_{1.5}}(x, y) = k_M^{1.5}(\|x - y\|_2 / \sigma_{\text{MMD}})$, respectively, with tunable bandwidth hyperparameter σ_{MMD} defining the length-scale of a feature. We then define the squared-exponential and Matèrn kernel functions respectively as

$$k_S(t) = \exp(-t^2/2), \quad k_M^\nu(t) = \frac{2^{1-\nu}}{\Gamma(\nu)} \left(\sqrt{2\nu}t\right)^\nu \kappa_\nu\left(\sqrt{2\nu}t\right),$$

with κ_ν as the modified ν -th Bessel’s function of the second kind, where we use $\nu = 1.5$ for this article. As it is infinitely differentiable, the MMD_{K_S} tends to be able to only identify broader features and “smooths out” distances, which makes it good for identifying when we want to check for the correct broad behavior. On the other hand, kernel function k_M^ν is only once differentiable for $\nu = 1.5$ at 0 and thus $\text{MMD}_{K_{M_{1.5}}}$ tends to reflect how well π and $\tilde{\pi}$ match higher-frequency features [71]. We also use the simpler error metrics of

$$d_{\text{RMSE}}^2(\pi, \tilde{\pi}) = \|\mathbb{E}_\pi[\theta] - \mathbb{E}_{\tilde{\pi}}[\theta]\|_2^2, \quad d_F^2(\pi, \tilde{\pi}) = \sum_{i=1}^d \ln^2 \lambda_i(\text{Cov}[\pi], \text{Cov}[\tilde{\pi}]),$$

where $\text{Cov}[\mu]$ is the covariance matrix of pdf μ and $\lambda_i(\mathbf{A}, \mathbf{B})$ is the i th-largest generalized eigenvalue of \mathbf{A} and \mathbf{B} . These are the RMSE and Förstner [36] distances. All discrepancies described are nominally semi-metrics (i.e., zero error in all of these is necessary but not sufficient for $\pi \equiv \tilde{\pi}$). For each example, we report each error relative the prior, e.g., for posterior π_M and j -th approximation $\tilde{\pi}_j$, we report $\tilde{D}(\pi_M, \tilde{\pi}_j) = D(\pi_M, \tilde{\pi}_j) / D(\pi_M, \pi_\theta)$ for distance D as each of the RMSE, Förstner, MMD_{K_S} and $\text{MMD}_{K_{M_{1.5}}}$ discrepancies. Since we learn $\tilde{\pi}$ via measure transport, this is intended to non-dimensionalize the errors relative to “how much work we would have to do to make d zero going from prior to posterior.” In other words, if $D(\pi, \pi_\theta) = \varepsilon > 0$, then we certainly would require $D(\pi, \tilde{\pi}) < \varepsilon$ to consider the method successful.

Notably, all of these require us to integrate over both $\tilde{\pi}$ and π . For D_{RMSE} and D_F , we measure the error between the moment of the true π_M and the estimated moments from normalized importance samples at step j , i.e., $(\theta_j^{(k)}, w_j^{(k)})_{k=1}^{N_j}$, using covariance estimation formula

$$\text{Cov}[\pi_j] \approx \frac{1}{1 - \sum_{k=1}^N (w_j^{(k)})^2} \sum_{k=1}^N w_j^{(k)} (\theta_j^{(k)} - \hat{\mu}_j)(\theta_j^{(k)} - \hat{\mu}_j)^\top, \quad \hat{\mu}_j = \sum_{k=1}^N w_j^{(k)} \theta_j^{(k)}.$$

To integrate with respect to a given unnormalized posterior density $\pi = \pi^{y^*} \pi_\theta \propto \pi$, we choose a fine-grid quadrature $(\theta_\pi^{(k)}, \tilde{w}_\pi^{(k)})_{k=1}^N$ on π_θ and then reweight according to $w_\pi^{(k)} \propto \pi^{y^*}(\theta_\pi^{(k)}) \tilde{w}_\pi^{(k)}$, where the proportionality comes from normalization of $\sum_k w_\pi^{(k)} \equiv 1$. For transport based $\tilde{\pi} = S^\# \eta$, we calculate MMD-based errors via a fine-grid pullback of quadrature rule $(z_\eta^{(k)}, w_\eta^{(k)})_{k=1}^N$ on η via $\theta_\eta^{(k)} = S^{-1}(z_\eta^{(k)})$.

Appendix G. Setup for numerical experiments. For all experiments, we use continuous Galerkin discretizations with structured uniform meshes. For all two-dimensional examples the MMD, RMSE, and Förstner calculations use an order 50 tensorized Gauss–Legendre quadrature rule (i.e., requiring 2500 evaluations of π), where the MMD bandwidth is $\sigma_{\text{MMD}} = 0.05$. Below are specific choices for each example.

Diffusion PDE single source inversion. We use first-order triangular elements with second-order quadrature for all solvers, where the data is generated with 256^2 elements. Likelihood $\pi_\ell^{y^*}$ has $(2m_\ell)^2$ elements for $m_0 = 8$, $m_1 = 32$, and $m_2 = 64$.

Diffusion PDE multi-source inversion. We use 256^2 second-order triangular elements with fourth-order quadrature for the data generation. Likelihood $\pi_\ell^{y^*}$ uses $(2m_\ell)^2$ first-order elements with second-order quadrature, where $m_0 = 8$, $m_1 = 16$, and $m_2 = 64$.

Convection diffusion reaction. We semi-discretize using first-order triangular elements with second-order quadrature for all solvers, where the data is generated with 256^2 elements and convection speed $c^* = 0.5$. All likelihoods $\pi_\ell^{y^*}$ use 32^2 elements, with differing convection speed c_ℓ , where $c_0 = 0$, $c_1 = 0.25$, and $c_2 = c^*$. These semi-discretizations are all solved using backward Euler on $t \in [0, 10]$ with $\Delta t = 0.1$ using a first-order BDF implicit solver. All MMD calculations use a bandwidth $\sigma = 0.1$ and the first $d^7 = 16,384$ four-dimensional Sobol’ points for the quadrature. The KDEs in Figures 8 and 9 are estimated using these 16384 Sobol’ points with a squared-exponential kernel, bandwidth calibrated according to $\sigma_{\text{KDE}} N^{-1/6}$, and σ_{KDE} as the average marginal standard deviation across all dimensions. For each subplot in Figures 8 and 9, the contour colors are calibrated as identical and the vertical scaling for the KDEs on the diagonal are identical.

Helmholtz. We use quadrilateral second-order elements with fourth-order quadrature for the solvers, where the data is generated using 128^2 elements and the (single) likelihood uses 64^2 elements.

Appendix H. Numerical comparisons. Here we describe and justify our comparisons in Section 5. In Subsection 5.3, we suggest that the Monte Carlo standard error for the mean would be approximately 3.42×10^{-2} when using $N = 75$ samples. This is derived using the 50^2 -point Gauss–Legendre quadrature rule to estimate the variance σ_j of each marginal j . We then recall the Lindeberg–Lévy central limit theorem: if $\bar{\Theta}$ is a sample mean of random variable Θ with mean μ and variance σ^2 , then the law of $\sqrt{n}(\bar{\Theta} - \mu)$ converges to a centered normal distribution with variance σ^2 . Using the Monte Carlo standard error of σ/\sqrt{N} , then, gives the 3.42×10^{-2} for each marginal (where each marginal has $\sigma \approx 0.296$).

In Subsection 5.5, we compare our method to SMC [24] and MCMC [42]. The first algorithm, Waste-Free SMC, is built on a sequence of tempered densities on which one performs Metropolis-like steps when performing SMC resampling. The “waste-free” nomenclature refers to the limiting of waste *inside* the metropolization; the entire algorithm, however, does not necessarily make use of every evaluation in the final produced set of weighted samples. This explains why, in Table 5, the algorithm produces 400 samples but requires 832 evaluations. The implementation was provided by the `particles` package [16], where we use the default adaptive tempering scheme with 25 particle ensembles and length 16 chains (the product of these two choices explains the size-400 rule). Similarly, the stretch MCMC algorithm [42] produces an interacting set of “walkers” (each of which produces a Markov chain), but does not necessarily use tempering or simulated annealing by default. We use 20 walkers with length 120 chains in UQPy [75], with a burn-in of 10 evaluations and thinning the chain by a factor of 10. For both SMC and MCMC, we only count evaluations as proposals that fall in the hypercube domain—i.e., if the algorithm proposed evaluating outside $[0, 1]^2$, we do not count this toward the evaluation count in Table 5. Here, the rESS of SMC is 0.385 once the points are made

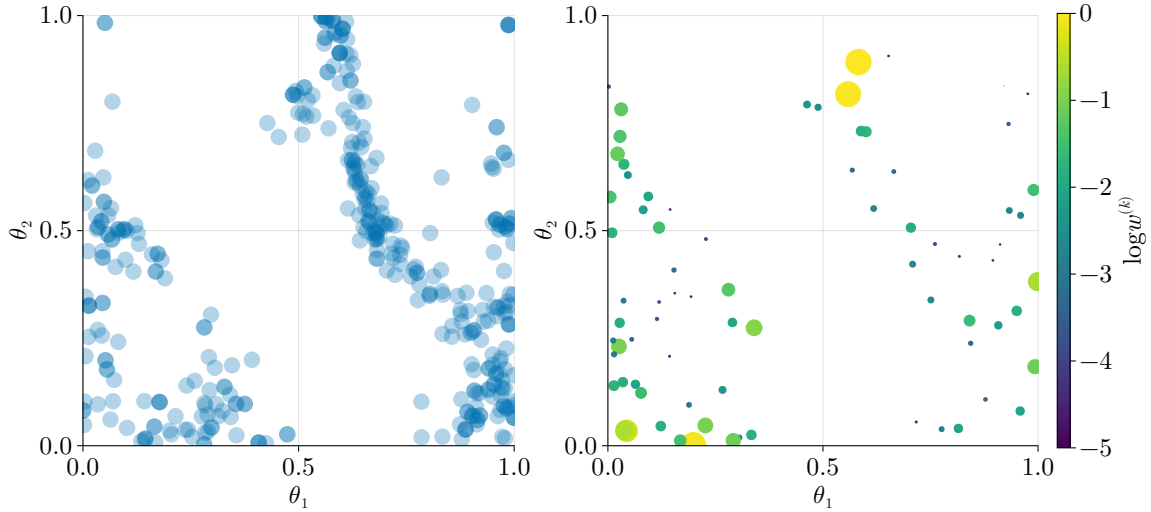


FIG. 12. Output quadratures of MCMC (left) and SMC (right). SMC marker size and color reflect the weight and log-weight of the sample point, respectively; MCMC is shown with opacity to demonstrate the rejections in the Markov chain.

uniquely (resulting in 79 points out of the original 400 samples); the rESS of MCMC of the original chains (before thinning) average about

$$(H.1) \quad \mathbb{E}_{\text{chains}} \left[\frac{1}{1 + 2 \sum_{k=1}^{\infty} \rho_k} \right] \approx (0.03833, 0.04078),$$

with an acceptance rate of 0.3121 averaged across the chains. Here, we estimate the length- k autocorrelation ρ_k for $0 \leq k \leq 30$, and each output corresponds to the rESS of each dimension.

We visualize the resulting quadratures of the SMC and MCMC in Figure 12. For reference, compare these to Figure 11, top left. Finally, for comparing the quadrature rules to one another we use the *sample-based* MMD calculation (with identical MMD bandwidth as in Section G). Given normalized quadrature rules Q_1 and Q_2 , the sample-based MMD is calculated as

$$(H.2) \quad \text{MMD}^2(Q_1, Q_2) = \overline{K}(Q_1, Q_1) - 2\overline{K}(Q_1, Q_2) + \overline{K}(Q_2, Q_2)$$

$$\overline{K}(Q, U) = \sum_{k=1}^{N_Q} \sum_{k'=1}^{N_U} K(\theta^{(k)}, \nu^{(k')}) w^{(k)} u^{(k')} \quad \text{with } Q = (\theta^{(k)}, w^{(k)})_{k=1}^{N_Q}, U = (\nu^{(k)}, v^{(k)})_{k=1}^{N_U}.$$